12-1-2003

I-Girders with Flange Rotational Restraint Braces

Richard Sause

Zhuo Fan

Clyde W. Ellis

Bong-Gyan Kim

I-Girders with Flange Rotational Restraint Braces

Work Area 5
Pennsylvania Innovative High Performance Steel
Bridge Demonstration Project

Report to
Commonwealth of Pennsylvania
Department of Transportation
Contract No. 359810

by

Richard Sause, Zhuo Fan,
Clyde W. Ellis, and Bong-Gyun Kim

ATLSS Report No. 03-22

December 2003

ATLSS is a National Center for Engineering Research
on Advanced Technology for Large Structural Systems

117 ATLSS Drive
Bethlehem, PA 18015-4729

Phone: (610)758-3525
Fax: (610)758-5902

www.atlss.lehigh.edu
Email: inatl@lehigh.edu

Technical Report Documentation Page

1. Report No.	2. Government Accession No.	3. Recipient's Catalog No.
FHWA-PA-2004-005-98-10 (e)		

4. Title and Subtitle	5. Report Date
I-Girders with Flange Rotational Restraint Braces: Work Area 5, Pennsylvania Innovative High Performance Steel Bridge Demonstration Project	December 2003 **6. Performing Organization Code** 4D371 (CAGE)
7. Author(s) Richard Sause, Zhuo Fan, Clyde W. Ellis, and Bong-Gyun Kim	**8. Performing Organization Report No.** ATLSS Report No. 03-22
9. Performing Organization Name and Address Advanced Technology for Large Structural Systems (ATLSS) Center Lehigh University 117 ATLSS Drive Bethlehem PA 18015-4729	**10. Work Unit No. (TRAIS)** **11. Contract or Grant No.** 359810
12. Sponsoring Agency Name and Address The Pennsylvania Department of Transportation Bureau of Planning and Research Commonwealth Keystone Building 400 North Street, 6th Floor Harrisburg, PA 17120-0064	**13. Type of Report and Period Covered** Final Report **14. Sponsoring Agency Code**

15. Supplementary Notes
COTR: Thomas P. Macioce

See Report Nos.: FHWA-PA-2004-005-98-10 (a), (b), (c), and (d) for related work.

16. Abstract
The Pennsylvania Department of Transportation (PennDOT) has proposed to design and construct a high performance steel demonstration bridge using HPS-485W (HPS-70W) steel in combination with I-shaped girders with corrugated webs. Toward this goal, a coordinated program of design and fabrication studies, and applied laboratory research (testing and analysis) has been conducted to develop details and design criteria for the bridge. This program, titled the "Pennsylvania High Performance Steel Bridge Demonstration Project", consisted of the following Work Areas: (1) corrugated web girder corrugation shape and strength criteria; (2) corrugated web girder fabrication; (3) fatigue resistance of corrugated web girders; (4) corrugated web girder field splices; and (5) diaphragms with flange rotational restraint braces. This report addresses Work Area 5, diaphragms with flange rotational restraint braces.

The scope of the report is summarized as follows: An analysis method for calculating the lateral-torsional buckling moment capacity of I-girders having diaphragms with flange rotational restraint braces is presented. The results of a large-scale test of a two-girder test specimen having diaphragms with flange rotational restraint braces are also presented. The properties of the test specimen are summarized, and the lateral-torsional buckling analysis method is used to analyze the test specimen. The test set-up, instrumentation, and test procedure are also summarized. The test results are presented and the analysis results are compared with the test results. Finally, the behavior of the test specimen is compared with the behavior assumed by the analysis method.

17. Key Words	18. Distribution Statement
Steel bridge, steel bridge girder, steel bridge girder bracing, lateral torsional stability, high performance steel	No restrictions. This document is available from the National Technical Information Service, Springfield, VA 22161 or by request to the PennDOT Research Program.

19. Security Classif. (of this report)	20. Security Classif. (of this page)	21. No. of Pages	22. Price
Unclassified	Unclassified	48	

I-Girders with Flange Rotational Restraint Braces

Work Area 5
Pennsylvania Innovative High Performance Steel
Bridge Demonstration Project

Report to
Commonwealth of Pennsylvania
Department of Transportation
Contract No. 359810

by

Richard Sause, Ph.D.
Professor of Structural Engineering
Lehigh University

Zhuo Fan
Graduate Research Assistant
Lehigh University

Clyde W. Ellis
Formerly, Graduate Research Assistant
Lehigh University

Bong-Gyun Kim
Graduate Research Assistant
Lehigh University

ATLSS Report No. 03-22

December 2003

ATLSS is a National Center for Engineering Research
on Advanced Technology for Large Structural Systems

117 ATLSS Drive
Bethlehem, PA 18015-4729

Phone: (610)758-3525
Fax: (610)758-5902

www.atlss.lehigh.edu
Email: inatl@lehigh.edu

Acknowledgements

This work was sponsored by the Pennsylvania Department of Transportation. Support was also provided by the Federal Highway Administration and the Pennsylvania Infrastructure Technology Alliance (funded by a grant from Pennsylvania Department of Community and Economic Development).

The Pennsylvania High Performance Steel Bridge Demonstration Project is a partnership of the ATLSS Center at Lehigh University with Drexel University (M. Elgaaly), High Steel Structures, Inc. (S. Kopp, R. Kase), and Modjeski and Masters, Inc. (W. Wassef), and involves many individuals (the primary contacts are given in parentheses). This report addresses Work Area 5 of this project. The test specimen described in the report was fabricated by High Steel Structures, Inc. The authors are grateful for the contributions of the technical staff of the ATLSS Center and Fritz Engineering Laboratory.

The contents of this report reflect the views of the authors, who are responsible for the facts and accuracy of the data presented herein. The contents do not necessarily reflect the official views or policies of the Commonwealth of Pennsylvania at the time of publication. This report does not constitute a standard, specification or regulation.

Table of Contents

Section		Page
1.	Introduction	1
2.	Lateral-Torsional Buckling of Bridge I-Girders with FRRBs	3
2.1	Introduction	3
2.2.	Flange Rotational Restraint Brace Concept	3
2.3.	Advantages of FRRBs	4
2.4.	Analysis of Lateral-Torsional Buckling Resistance	4
2.5.	AASHTO LRFD Lateral-Torsional Buckling Resistance Formulas	6
2.6.	Inelastic Equation for Sections with Stocky Webs	7
2.7.	Estimating the Effective Length Factor, K_b	8
3.	Test Specimen	11
3.1.	Overview	11
3.2.	Test Specimen Dimensions	11
3.3.	Cross Frames and FRRBs	12
3.4.	As-Built Dimensions and Properties	12
3.5.	Calculated Lateral-Torsional Buckling Resistance of Test Specimen	12
4.	Test Set-up, Instrumentation, and Procedure	20
4.1.	Introduction	20
4.2.	Test Set-Up	20
4.3.	Instrumentation	20
4.4.	Test Procedure	21
5.	Test Results	27
5.1.	Introduction	27
5.2.	Applied Load	27
5.3.	Girder Top Flange Lateral Curvature	29
5.4.	FRRB Lateral Curvature	29
5.5.	Girder Top Flange Lateral Deflection	30
5.6.	Moment at Lateral-Torsional Buckling	31
5.7.	Comparison with Calculated Lateral-Torsional Buckling Resistance	32
5.8.	Comparison with Behavior Assumed by Analysis Method	32
6.	Summary and Conclusions	47
References		48

List of Tables

Table	Page
Table 1. Tension coupons test results	14
Table 2. Rotational stiffness parameters and effective length factors	14
Table 3. Calculated lateral-torsional buckling resistance of test specimen	14
Table 4. Major principle axis bending moment at load points and at midspan	33
Table 5. Calculated lateral-torsional buckling resistance of test specimen	33

List of Figures

Figure		Page
Figure 1.	FRRB used in test specimen	9
Figure 2.	Frame structure deflected shape	9
Figure 3.	Model for I-girder with FRRBs	10
Figure 4.	Lateral deflected shapes for unbraced length of compression flange	10
Figure 5.	Test specimen girders	15
Figure 6.	Test specimen girder and FRRB nominal cross section dimensions	16
Figure 7.	Test specimen cross frames	17
Figure 8.	FRRB connection details	17
Figure 9.	As-built test specimen girder cross section dimensions	18
Figure 10.	As-built test specimen girder dimensions	19
Figure 11.	Test set-up	22
Figure 12.	Test set-up elevation view near intermediate cross frames	23
Figure 13.	Photograph of test set-up	23
Figure 14.	Schematic of hydraulic pump and manifold system	24
Figure 15.	Photograph of hydraulic actuator with pressure transducer PT1	24
Figure 16.	Deflection, rotation, and reaction instrumentation	25
Figure 17.	Strain gage sets	26
Figure 18.	Photograph of actuator calibration	34
Figure 19.	Load from pressure transducer versus measured reactions	35
Figure 20.	Relationship between applied load and pressure in actuator	35
Figure 21.	Photograph of north girder at peak load	37
Figure 22.	Photograph of north girder after peak load.	38

List of Figures (continued)

Figure	Page
Figure 23. Load versus midspan vertical deflection	39
Figure 24. Girder top flange lateral curvature ($x10^{-6}$/in) at different load levels	40
Figure 25. FRRB lateral curvature ($x10^{-6}$/in) at different load levels	41
Figure 26. Girder top flange lateral deflection at different load levels	42
Figure 27. Girder top flange initial lateral deflection (out-of-straightness)	43
Figure 28. Girder top flange total lateral deflection at different load levels	44
Figure 29. Girder major axis bending moment at peak from Method 1	45
Figure 30. Girder major axis bending moment at peak from Method 2	46

Abstract

The Pennsylvania Department of Transportation (PennDOT) has proposed to design and construct a high performance steel demonstration bridge using HPS-485W (HPS-70W) steel in combination with I-shaped girders with corrugated webs. To assist PennDOT, a coordinated program of design and fabrication studies, and applied laboratory research (testing and analysis) has been conducted to develop details and design criteria for the bridge. This project, titled the "Pennsylvania High Performance Steel Bridge Demonstration Project", is being conducted by the following team: (1) the ATLSS Center at Lehigh University, (2) Modjeski and Masters, Inc., (3) High Steel Structures, Inc., and (4) Drexel University. The program consists of the following Work Areas: (1) corrugated web girder corrugation shape and strength criteria; (2) corrugated web girder fabrication; (3) fatigue resistance of corrugated web girders; (4) corrugated web girder field splices; and (5) precast deck and diaphragms with flange rotational restraint braces.

This report addresses Work Area 5, but addresses only I-girders having diaphragms with flange rotational restraint braces. The scope of the report is summarized as follows: An analysis method for calculating the lateral-torsional buckling moment capacity of I-girders having diaphragms with flange rotational restraint braces is presented. The results of a large-scale test of a two-girder test specimen having diaphragms with flange rotational restraint braces are also presented. The properties of the test specimen are summarized, and the lateral-torsional buckling analysis method is used to analyze the test specimen. The test set-up, instrumentation, and test procedure are also summarized. The test results are presented and the analysis results are compared with the test results. Finally, the behavior of the test specimen is compared with the behavior assumed by the analysis method.

1. Introduction

The Pennsylvania Department of Transportation (PennDOT) has proposed to design and construct a HPS demonstration bridge using HPS-485W (HPS-70W) steel in combination with innovative bridge design concepts. The site of the bridge is to be determined. The demonstration bridge will be a multiple steel I-girder bridge. The girders will be fabricated with corrugated webs, and may be braced with cross frames that include compression flange rotational restraint braces. Precast high-performance concrete panels may be used to construct the deck without extensive use of field-placed concrete. To assist PennDOT with the development of the demonstration bridge, a coordinated program of design and fabrication studies, and applied laboratory research (testing and analysis) has been conducted to develop details and design criteria for the bridge. This project, titled the "Pennsylvania High Performance Steel (HPS) Bridge Demonstration Project", is being conducted by a team composed of the following participants: (1) the ATLSS Center at Lehigh University, (2) Modjeski and Masters, Inc., (3) High Steel Structures, Inc., and (4) Drexel University.

The coordinated program of design and fabrication studies, and applied laboratory research (testing and analysis) consists of the following work areas: (1) corrugated web girder corrugation shape and strength criteria; (2) corrugated web girder fabrication; (3) fatigue resistance of corrugated web girders; (4) corrugated web girder field splices; (5) precast deck and diaphragms with flange rotational restraint braces.

This report addresses Work Area 5. During the course of the project, the studies in Work Area 1 showed that current corrugated web girder shear strength criteria and flexural strength theory were inadequate, and substantially new shear strength criteria and new flexural strength theory were developed in Work Area 1 (Sause *et al*. 2003). In addition, questions about the design of bearing stiffeners for corrugated web girders were raised, and a study of bearing stiffeners was undertaken within Work Area 4 (Sause and Clarke 2003). As a consequence of the additional effort required to complete Work Areas 1 and 4, Work Area 5 was limited to I-girders having diaphragms with flange rotational restraint braces. Therefore, this report addresses only I-girders having diaphragms with flange rotational restraint braces.

The work presented in this report builds on previous work at the ATLSS Center at Lehigh University. Murphy (1997) first investigated the use flange rotational restraint braces (FRRBs) to improve the lateral-torsional stability of the top flanges of composite I-girders during the construction stage before the concrete deck is composite with the I-girders. Ellis and Sause (1999) investigated specific modifications to bridge I-girder design practice to include the use of FRRBs. They studied the influence of changes in design parameters and the trade off between reductions in I-girder weight and reductions in I-girder fabrication effort, including using FRRBs.

The present report covers two main areas of work. First, an analysis approach for I-girders with cross frames and FRRBs initially suggested by Murphy (1997) is reviewed and improved. The method was applied to a test specimen that was designed specifically for tests of the FRRB bracing concept. Second, experiments on the test specimen consisting of two I-girders braced by diaphragms (specifically, cross frames) with FRRBS are presented. The properties of the test specimens, instrumentation, and test procedures are presented, and the test data is analyzed. The test results and

analysis results are compared, and the behavior of the test specimen is compared with the behavior assumed by the analysis method.

The remainder of the report is organized as follows. Section 2 reviews the lateral-torsional buckling of bridge I-girders, and the FRRB concept. An analysis method for determining the lateral-torsional buckling moment for I-girders with FRRBs is presented. Section 3 describes the properties of the test specimen, and the lateral-torsional buckling analysis method is used to analyze the test specimen. Section 4 presents the test set-up, instrumentation, and test procedure. Section 5 presents an analysis of the test results. The lateral-torsional buckling analysis results for the test specimen are compared with the test results and the behavior of the test specimen is compared with the behavior assumed by the analysis method. Section 6 summarizes the study discussed in the report.

2. Lateral-Torsional Buckling of Bridge I-Girders with FRRBs

2.1. Introduction

To make bridge I-girders economical, the moment of inertia about the major principle axis, *x*, is considerably larger than that about the minor principle axis, *y*. In addition, I-girders are open sections, which are inefficient in resisting torsion. Therefore, when bending about the *x*-axis introduces lateral bending about the *y*-axis or torsion due to geometric imperfections and unintended eccentricities, significant lateral deflection or twist can develop. When lateral deflection and twist increase suddenly resulting in a decrease in the *x*-axis bending resistance, the behavior is called lateral-torsional buckling. Lateral-torsional buckling is usually resisted by compression flange bracing. In this section, the use of flange rotational restraint braces (FRRBs) to brace the compression flange is introduced. Lateral-torsional buckling theory is reviewed, and lateral-torsional buckling formulas and the application of these formulas to I-girders braced with FRRBs are presented.

2.2. Flange Rotational Restraint Brace Concept

In practice, lateral-torsional buckling of bridge steel I-girders is prevented by bracing the compression flange. For positive moment regions of composite I-girders, the top (compression) flange is braced by the deck and further bracing is not needed during the service stage. However, during the construction stage, before the concrete deck is composite with the girders, girder lateral-torsional buckling under construction loads is possible, and thus bracing is needed. In addition, near the piers of continuous span bridges, the I-girder bottom flange will be in compression due to negative bending. Under this condition, bracing of bridge I-girders is needed even when the top flange is composite with the deck.

This report focuses on a specific type of compression flange brace, first presented by Murphy (1997), called a “flange rotational restraint brace”, or FRRB. An FRRB consists of a plate or a wide flange T-beam rigidly attached to the compression flange of an I-girder at the location of a standard cross frame (see Figure 1). A cross frame is located below the FRRB to brace the cross section against lateral displacement and twist. The FRRB restrains the rotation of the compression flange in its own plane, and thereby further restrains, indirectly, the lateral deflection of the compression flange.

A system of I-girder compression flanges with FRRBs and associated cross frames is similar to a frame structure in which the beams restrain the column rotations. This restraint by the beams reduces the effective length of the columns. When the beams are connected to the columns with pinned connections (Figure 2(a)), the effective length of the column L_{eff} is equal to the story height H, that is, $L_{eff} = H$. When the beams are rigidly connected to the columns (Figure 2(b)), the effective length of the columns is reduced. If the beams are flexurally rigid, the column effective length is half the story height, that is $L_{eff} = 0.5H$. The reduced column effective length increases the column buckling capacity. For I-girders braced with FRRBs and cross frames, the compression flanges are similar to columns in compression with beams restraining their rotation. The FRRBs are similar to the beams, restraining the compression flange rotation and reducing the effective unbraced length of the flange. An effective length factor K_b can be used to quantify this effect of FRRBs.

FRRBs function like a rotational spring to resist the rotation of the compression flange. Thus, a simplified model of a compression flange braced with FRRBs is a compression element laterally braced by roller supports (*i.e.*, the cross frames) and rotationally restrained by the FRRBs (Figure 3). The effective length factor, K_b, quantifies the effect of the rotational spring. When the compression flange is braced with cross fames without FRRBs (*i.e.*, the rotational springs have no stiffness), and K_b is equal to 1. The buckling deflected shape of an unbraced length of the compression flange is shown in Figure 4(a). Here we assume all unbraced lengths of the compression flange buckle at the same time, and only one unbraced length is shown. When cross frames with FRRBs are used, K_b is equal to 0.5 if the FRRBs are rigid (*i.e.*, the rotational springs are rigid). For more realistic cases, K_b will fall into the range of 0.5 to 1. The buckling deflected shape of an unbraced length is shown in Figure 4(b). Figure 4 shows the lateral deflected shape with FRRBs has less rotation at the ends of the unbraced length and the lateral curvature reverses within the unbraced length due to the rotational restraint of the FRRBs. The lateral deflected shape with FRRBs also has three points of inflection in the lateral deflected shape of the compression flange near the FRRB. Murphy (1997) shows that the rotational stiffness of the spring modeling the FRRB can be estimated as:

$$k_\theta = \frac{2E_f I_{yf}}{L_s} \tag{1}$$

where,

E_f is the modulus of elasticity of the FRRB,
I_{yf} is moment of inertia of the FRRB about the vertical axis,
L_s is the girder spacing from center to center.

2.3. Advantages of FRRBs

The primary advantage of FRRBs is the possibility of increasing the cross frame spacing without decreasing the lateral-torsional buckling moment capacity of bridge I-girders. The restraint from the FRRBs reduces the effective unbraced length of the I-girder flanges, and thus the lateral-torsional buckling capacity is increased with a given unbraced length. Therefore, the lateral-torsional buckling capacity of I-girders for a given unbraced length without FRRBs can be maintained while the unbraced length is increased, if FRRBs are included.

The practical benefits from using FRRBs are as follows. Cross frames and cross frame connections are expensive, and the total cost of the cross frames and their connections can be decreased by reducing the number of cross frames. The fatigue performance of bridge I-girders can be improved by eliminating cross frames and the associated connection plates. Alternately, if the cross frames are located at high stress locations, less economical connection plate details with better fatigue resistance can be used effectively because there are fewer cross frames.

2.4. Analysis of Lateral-Torsional Buckling Resistance

The differential equations for I-girder lateral-torsional buckling are (Galambos 1968):

$$EI_y u^{iv} + M_x \varphi'' + 2 M_x' \varphi' = 0 \tag{2a}$$

$$EI_w \varphi^{iv} - (GJ + M_x \beta_x)\varphi'' - M_x' \beta_x \varphi' + M_x u'' = 0 \tag{2b}$$

where,

E is the modulus of elasticity,
G is the shear modulus,
J is the torsion constant,
I_y is the moment of inertia about the minor principle axis, y,
I_w is the warping moment of inertia,
β_x is the monosymmetry section property,
u is the lateral deflection of the shear center,
φ is the angle of cross section twist about the shear center,
M_x is the moment about the major principle axis x,
M_x' is the moment gradient.

When the I-girder is in the state of pure bending, the moment gradient M_x' is zero, and the moment M_x at any cross section of the I-girder is constant, i.e., $M_x = M_0$. In this case the differential equations for lateral-torsional buckling of an I-girder are:

$$EI_y u^{iv} + M_0 \varphi'' = 0 \tag{3a}$$

$$EI_w \varphi^{iv} - (GJ + M_0 \beta_x) \varphi'' + M_0 u'' = 0 \tag{3b}$$

The monosymmetry section property β_x for I-girders can be expressed in terms of the section dimensions and the coordinates of the shear center as follows (Galambos 1968):

$$\beta_x = \frac{1}{I_x}\left\{(d' - \bar{y})\left[\frac{b_t^3 t_t}{12} + b_t t_t (d' - \bar{y})^2 + (d' - \bar{y})^3 \frac{t_w}{4}\right] - \bar{y}\left(\frac{b_c^3 t_c}{12} + b_c t_c \bar{y}^2 + \bar{y}^3 \frac{t_w}{4}\right)\right\} - 2y_0$$

where,

b_t , t_t are the width and thickness of the tension flange respectively,
b_c , t_c are the width and thickness of the compression flange respectively,
t_w is the web thickness,
d' is the distance between the flange centroids,
$\bar{y}$ is the distance between the section centroid and compression flange centroid,
y_0 is the distance between the section shear center and section centroid.

For a doubly symmetric cross section, β_x is equal to zero.

The lateral-torsional buckling moment can be obtained by solving the differential equations of Equations 2a and 2b or Equations 3a and 3b. The results will depend on the specified boundary conditions. For an I-girder with cross frames, the boundary conditions of an unbraced length, L_b, are assumed simply supported at the location of the cross frames. The lateral deflection and twist are restrained, but warping and lateral bending are assumed to be free:

$$u = \varphi = u'' = \varphi'' = 0 \tag{4}$$

Assuming the section is doubly symmetric, and the moment is uniform over the unbraced length, the solution of Equations 3a and 3b is (Galambos 1968):

$$M_{cr} = \frac{\pi}{L_b}\sqrt{EI_y GJ\left(1 + \frac{\pi^2 EI_w}{GJL_b^2}\right)} \tag{5}$$

For an I-girder with cross frames and FRRBs, the boundary conditions are different from Equation 4. At the locations of the FRRBs, the cross frames provide support against the lateral deflection and twist. The FRRBs are similar to rotational springs that restrain the in-plane rotation of the compression flange. Thus, the sections at the locations of the cross frames with FRRBs are restrained against lateral deflection and twist by the cross frames and are partially restrained against warping and lateral bending by the FRRBs.

Differential equations with these boundary conditions are difficult to solve in closed form. Thus, numerical procedures are needed to solve the equations, such as the finite element method or the finite difference method, as discussed by Murphy (1997). In this report, the lateral-torsional buckling formulas of the AASHTO LRFD bridge design specifications (AASHTO 1998) will be used to analyze I-girders with FRRBs.

2.5. AASHTO LRFD Lateral-Torsional Buckling Resistance Formulas

The AASHTO LRFD bridge design specifications (AASHTO 1998) provide formulas for the lateral-torsional buckling resistance that are derived from Equation 5. The following approximations are made:

$$I_y = 2\ I_{yc} \tag{6a}$$

$$I_w = ½\ (I_{yc}\ d^2) = ¼\ (I_y\ d^2) \tag{6b}$$

Where, d is the depth of the cross section. The compression flange moment of inertia about the y-axis is assumed to be approximately equal to that of the tension flange. The moment of inertia of the web about the y-axis is neglected. Using these two approximations of Equation 6 results in the following:

$$M_{cr} = \frac{\pi\ EI_{yc}}{L_b}\sqrt{\frac{2GJ}{EI_{yc}} + \frac{\pi^2 d^2}{L_b^2}} \tag{7}$$

With π = 3.14, $2G/E$ = 0.772, π^2 = 9.87, Equation 7 becomes:

$$M_{cr} = \frac{3.14EI_{yc}}{L_b}\sqrt{\frac{0.772J}{I_{yc}} + \frac{9.87d^2}{L_b^2}} \tag{8}$$

Equation 8 is the AASHTO formula for the lateral-torsional buckling moment capacity of an I-girder with a stocky web. For an I-girder with a slender web, the term with the torsion constant J is omitted. For an I-girder with FRRBs, the effective unbraced length K_bL_b is used in place of L_b as shown below. For an unbraced length with a moment gradient, the moment gradient factor, C_b, is included as shown below.

The web slenderness, $2D_c/t_w$, is used to determine if the web is stocky or slender, where D_c is the depth of the web in compression. When $2D_c/t_w \le (\lambda_b(E/F_{yc})^{1/2})$ the I-girder cross section is categorized as a stocky web section. For elastic lateral-torsional buckling, the moment capacity of a stocky web section is:

$$M_{cr} = \frac{3.14C_bR_hEI_{yc}}{K_kL_b}\sqrt{\frac{0.772J}{I_{yc}} + \frac{9.87d^2}{(K_bL_b)^2}} \tag{9}$$

where,

λ_b is a coefficient (see AASHTO 1998),
F_{yc} is the yield stress of the compression flange,
C_b is the moment gradient correction factor,
R_h is the flange stress reduction factor for a hybrid cross section.

For I-girders with stocky webs, an inelastic lateral torsional buckling formula for stocky web is not included in the AASHTO LRFD specifications. This issue will be addressed in the following subsection of the report.

When $2D_c / t_w \geq (\lambda_b(E / F_{yc})^{1/2})$ the I-girder cross section is categorized as a slender web cross section. For a slender web cross section, cross section distortion is likely and the torsion constant J is taken as 0. If $KL_b \geq L_r$, the lateral-torsional buckling capacity is the elastic lateral-torsional buckling moment, and if $KL_b \leq L_r$ the lateral-torsional buckling capacity is the inelastic lateral-torsional buckling moment. For an I-girder with a slender web cross section, L_r is as follows:

$$L_r = 4.44((I_{yc}\, d\, E) / (S_{xc}F_{yc}))^{1/2} \tag{10}$$

where, S_{xc} is the section modulus to the compression flange. The elastic lateral-torsional buckling moment is:

$$M_n = C_b R_b R_h (0.5 M_y) \left(\frac{L_r}{K_b L_b} \right)^2 \leq R_b R_h M_y \tag{11}$$

where, R_b is the flange stress reduction factor for web bend buckling (AASHTO 1998), and M_y is the compression flange yield moment. The inelastic lateral-torsional buckling moment is:

$$M_n = C_b R_b R_h M_y \left(1 - 0.5 \left[\frac{K_b L_b - L_p}{L_r - L_p} \right] \right) \leq R_b R_h M_y \tag{12}$$

where, $L_p = (1.76 r_t (E / F_{yc})^{1/2})$ and r_t is a radius of gyration of the compression flange and a portion of the web (AASHTO 1998).

2.6. Inelastic Equation for Sections with Stocky Webs

As noted above, an inelastic lateral torsional buckling formula for stocky web I-girders is not included in the AASHTO LRFD specifications (AASHTO 1998). A straight line transition is used in the present study to determine the inelastic lateral-torsional buckling moment for an I-girders with a stocky web. If $KL_b \geq L_r$, the lateral-torsional buckling capacity is the elastic lateral-torsional buckling moment given by Equation 9. If $KL_b \leq L_r$ the lateral-torsional buckling capacity is the inelastic lateral-torsional buckling moment given below. For a stocky web I-girder, L_r is as follows:

$$L_r = \sqrt{\frac{4\pi^2 E I_{yc}}{M_y^2} \left(GJ + \sqrt{(GJ)^2 + \left(\frac{d \cdot M_y}{2} \right)^2} \right)} \tag{13}$$

The inelastic lateral-torsional buckling moment is:

$$M_n = C_b R_h M_y \left(1 - 0.5\left[\frac{K_b L_b - L_p}{L_r - L_p}\right]\right) \le R_h M_y \tag{14}$$

The above formulas from the AASHTO specifications and this straight line transition for stocky web sections, including K_b, are referred to as the lateral-torsional buckling formulas with K_b in the remainder of the report.

2.7. Estimating the Effective Length Factor, K_b

As noted above, the lateral-torsional buckling moment capacity of steel I-girders with FRRBs can be determined using the finite element method or the finite difference method, as shown by Murphy (1997). In the present study, an effective length factor, K_b, is introduced into the lateral-torsional buckling resistance formulas of the AASHTO LRFD specifications, and these lateral-torsional buckling formulas with K_b are used to determine the lateral-torsional buckling moment capacity of steel I-girders with FRRBs. In this section, a so-called "alignment" chart method is introduced to calculate the effective length factor K_b.

To use the alignment chart, the rotational stiffness parameters Ψ_i and Ψ_j are calculated at the locations where the compression flange is braced by the FRRBs. The rotational stiffness parameter reflects the restraint of the FRRBs on the compression flange. From the values of Ψ_i and Ψ_j, the value of K_b is determined from a standard alignment chart (*e.g.*, see Salmon and Johnson 1971). Ψ_i and Ψ_j are calculated as follows:

$$\psi = \frac{\sum((E \cdot I_{yc})/L_b)}{\sum((E \cdot I_y^{FRRB})/L_s)} \tag{15}$$

where, L_s is the spacing between girders, and I_y^{FRRB} is the moment of inertia of the FRRB flange. The summation in the numerator is over the number of unbraced lengths that meet at the cross frame location, and the summation in the denominator is over the number of FRRBs attached to each I-girder at the cross frame location.

Equation 15 can be simplified as follows if only one FRRB is attached to the girder at cross frame location and the moment of inertia of the compression flange is constant:

$$\psi = \frac{I_{yc} L_s}{I_y^{FRRB}}\left[\frac{1}{L_{bm}} + \frac{1}{L_{bn}}\right] \tag{16}$$

where, L_{bm} and L_{bn} are the two unbraced lengths that meet at the cross frame location. With Ψ_i and Ψ_j determined, an alignment chart can be used to find the factor K_b. However, the following equation can be used to determine K_b with more accuracy (Salmon and Johnson 1971), and is used in the present study.

$$\frac{\psi_i \psi_j}{4}\frac{\pi^2}{K_b^2} + \left(\frac{\psi_i + \psi_j}{2}\right)\left(1 - \frac{\pi/K_b}{\tan \pi/K_b}\right) + \frac{2}{\pi/K_b}\tan\frac{\pi}{2K_b} = 1 \tag{17}$$

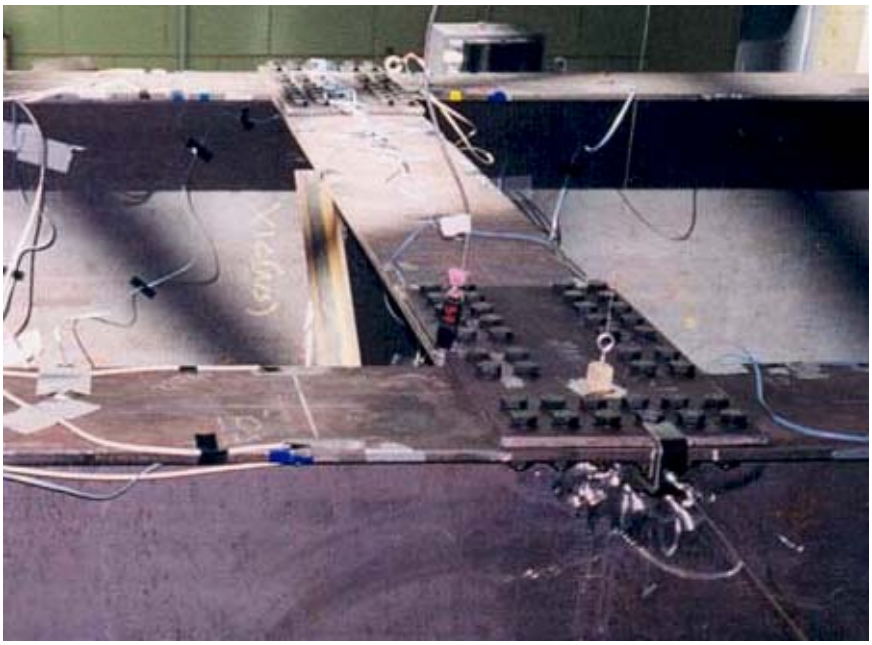

Figure 1. FRRB used in test specimen.

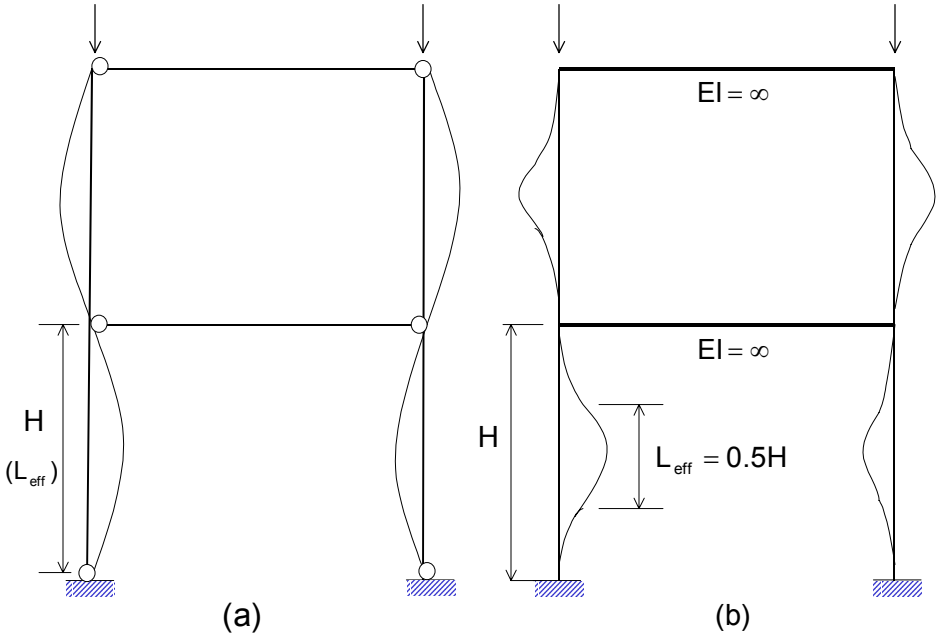

Figure 2. Frame structure deflected shape: (a) beams with pin connections, (b) rigid beams with rigid connections.

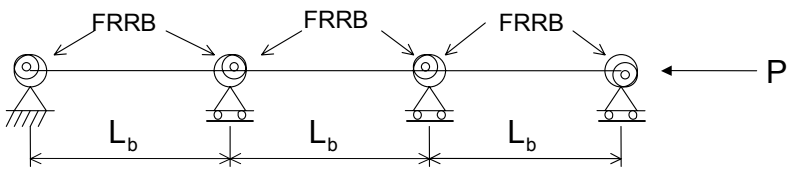

Figure 3. Model for I-girder with FRRBs.

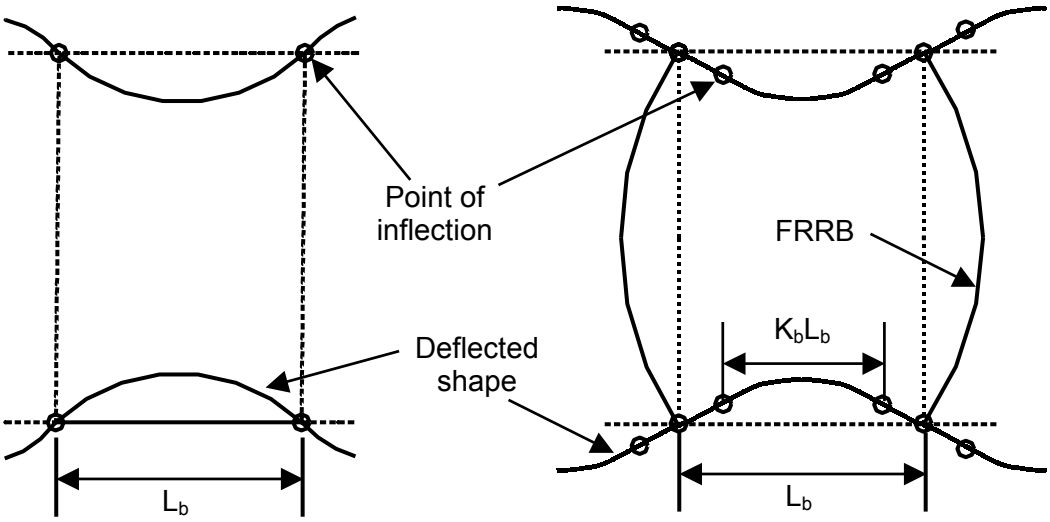

(a) With cross frames without FRRBs (b) With cross frames with FRRBs

Figure 4. Lateral deflected shapes for unbraced length of compression flange.

3. Test Specimen

3.1. Overview

The test specimen is based on I-girders and FRRBs designed for a prototype bridge by Ellis and Sause (1999). The prototype bridge is a simply supported single span bridge with no skew. It is 131.24ft long and 50ft wide. The bridge has two driving lanes and sidewalks. The bridge has four straight I-girders spaced at 12.5ft with 6.25ft overhangs. The four girders are braced by conventional cross frames at the ends (at the bearings) and two intermediate cross frames with FRRBs. The concrete deck is 10in thick. The bridge was designed according to the AASHTO LRFD bridge design specifications (AASHTO 1998), including the loading conditions and the limits states of strength, serviceability and fatigue. The girders were designed for HPS-70W steel with a nominal yield stress of 70ksi. The cross frame spacing and FRRBs were designed so that lateral-torsional buckling occurred in all three unbraced lengths at approximately the same load level in order to minimize the restraint against buckling that can be provided by adjacent unbraced lengths that are not buckling. The design details of the prototype bridge are given in Ellis and Sause (1999).

The test specimen consists of two of the four girders I-girders of the prototype bridge braced by cross frames. The two intermediate cross frames have FRRBs and the end cross frames do not. The test specimen was obtained by scaling the I-girders, cross frames, and FRRBs designed for the prototype bridge by one-half.

3.2. Test Specimen Dimensions

Each I-girder is divided into three unbraced lengths by the four cross frames of the test specimen. The unbraced lengths at the ends are called the east outer unbraced length and the west outer unbraced length, respectively. The middle unbraced length is called the inner unbraced length. The nominal span of the I-girders from centerline-to-centerline of the bearings is 65.61ft. The nominal outer unbraced length from the centerline of the bearing to the centerline of the intermediate cross frame connection plate is 23.79ft. The inner unbraced length from the centerlines of the two intermediate cross frame connection plates is 18.03ft. The nominal I-girder spacing is 6.25ft to the web centerlines. Figure 5 shows the nominal geometry of the test specimen I-girders.

The prototype bridge girders were designed with shop slices to reduce the I-girder weight. The two shop slices divide the girders into three segments. The segment between the end of the girders and the plate transitions are called the end segments. The cross section for this segment is called Section 1. The segment between the two plate transitions is called the middle segment. The cross section for this segment is called Section 2. The shop slices locations and segment lengths are shown in Figure 5. The figure shows that the shop splices fall in the outer unbraced lengths. The cross sections for Section 1 and Section 2 are shown in Figure 6.

The FRRBs are composed of a built-up T-section. The dimensions of the FRRB cross section are shown in Figure 6. The nominal length of the FRRBs is the nominal girder spacing of 6.25ft.

3.3. Cross Frames and FRRBs

The girders are braced by two end cross frames and two intermediate cross frames with FRRBs. The cross frames are designed to resist lateral-torsional buckling. The approach used to design the cross frames is given in Ellis and Sause (1999).

The cross frames are shown in Figure 7. For economical reasons, the intermediate and end cross frame members were designed using a limited number of angle sizes. The bottom chord is large enough to allow the diagonals to be welded to it. In this way, a gusset plate is eliminated. The top chord of the intermediate cross frames is the T-section FRRB described previously. The top chord of the end cross frames is a channel. The depth of the channel allowed enough space to weld the diagonals.

The cross frames are attached to the connection plates with ½in diameter A325 high strength bolts. As shown in Figure 7, there is an offset of 2in between the bottom chord and the bottom flange for both the intermediate cross frames and the end cross frames. The offset is 1-½in between the top flange and the top chord. As shown in Figure 8, the FRRB flange is connected to the I-girder top flange using a bolted splice connection plate (19-5/16in x 9-½in x ½in). The bolts are ½in diameter A325 high strength bolts. The FRRB web is bolted to the cross frame connection plate, as shown in Figure 8.

3.4. As-Built Dimensions and Properties

As noted earlier, the test specimen includes two I-girders, called the north girder and the girder respectively. The as-built girder spacing was 6.24ft. The as-built dimensions of the north and south girders have slight differences (see Figures 9 and 10). The as-built cross section dimensions are shown in Figure 9.

Tension coupons were tested to obtain the material properties of the test girder steel. Four tension coupons were fabricated from the top flange plate, with a thickness of ½in. Three were fabricated from the web plate, with a thickness of 5/16in. The test results of the coupons are shown in Table 1. The elastic modulus of the test specimen was taken as 30000ksi.

3.5. Calculated Lateral-Torsional Buckling Resistance of Test Specimen

As shown in Figure 5, the cross frames of the test specimen divide the I-girder compression flanges into three unbraced lengths, which are called L_{b1}, L_{b2}, and L_{b3}. The east intermediate cross frame, between L_{b1} and L_{b2}, has an FRRB, and the west intermediate cross frame, between L_{b2} and L_{b3}, has an FRRB. The rotational stiffness parameter at the east FRRB is Ψ_1, and the rotational stiffness parameter at the west FRRB is Ψ_2. The rotational stiffness parameters for the east end cross frame, Ψ_3, and the west end cross frame, Ψ_4, are both theoretically equal to ∞.

The as-built unbraced lengths for both the north and south girders of the test specimen are given in Table 2. Table 2 also gives the ratio I_{yc}/I_{yf}. This data was used with

Equation 16 to determine Ψ_1 and Ψ_2 each girder. For example, for the north girder, L_{b1} = 285.9in, L_{b2} =217.0in, and L_{b3} = 286.3in, I_{yc}/I_{yf} = 1.043, and L_s = 74.9in. The resulting values for Ψ_1 and Ψ_2 are both 0.633, which indicates that the small differences between L_{b1} and L_{b3} are inconsequential.

With these values for Ψ_1 and Ψ_2, and with Ψ_3 and Ψ_4 equal to ∞. Equation 17 was used to determine the effective length factor, K_b. For the inner unbraced length of the north girder, K_b = 0.716, and for the east and west outer unbraced lengths K_b = 0.839. Since $\Psi_1 = \Psi_2$ and $\Psi_3 = \Psi_4$, the two outer unbraced lengths have the same value of K_b.

Using the K_b values in Table 2, the lateral-torsional buckling moment capacity of the I-girders of the test specimen was calcuated. The as-built dimensions, compression (top) flange yield stress of 83.5 ksi from the coupon tests (Table 1), and an elastic modulus of 30000 ksi were used in the calculations.

The cross section of the end segments of the north and south I-girders, called Section 1, and the cross section of the middle segment, called Section 2, are both categorized as a stocky web cross sections. R_h = 1.0 because the cross sections are considered homogeneous.

The loading pattern applied to the test specimen (discussed in Section 4) produces a constant moment over the inner unbraced length, so the moment gradient factor, C_b = 1.0. In addition, $KL_b \leq L_r$ for the inner unbraced length, where L_r is calculated from Equation 13, so Equation 14 (for inelastic lateral torsional buckling) was used to determine the moment capacity. For the north girder (from Equation 14), M_n = 11,110 kip-in. The south girder is similar to the north girder, except the dimensions vary slightly. For the south girder (from Equation 14), M_n = 10,870 k-in.

As discussed in Section 3.2, the outer unbraced lengths have two different cross sections called Section 1 and Section 2. Also, the loading pattern applied to the test specimen (discussed in Chapter 4) produces a linear moment gradient over the outer unbraced lengths, with zero moment at the ends (at the bearings), so the moment gradient factor C_b should be calculated and used in the lateral torsional buckling moment formulas. The AASHTO LRFD specifications (AASHTO 1998) include two formulas for C_b. For this linear moment gradeint, C_{b1} = 1.67 and C_{b2} = 1.75 are obtained from the two formulas given in the AASHTO LRFD specifications. Finally, for the outer unbraced lengths, $KL_b \geq L_r$, so the lateral-torsional buckling capacity is the elastic lateral-torsional buckling moment given by Equation 9.

For the outer unbraced lengths of the north girder, using Section 1 as the cross section, M_n = 9424 k-in, when C_{b1} = 1.67 is used, and M_n = 9884 k-in when C_{b2} = 1.75 is used. With Section 2 as the cross section, M_n = 10160 k-in, when C_{b1} = 1.67 is used, and M_n = 10640k-in when C_{b2} = 1.75 is used.

The south girder is similar to the north girder, except the dimensions vary slightly. For the outer unbraced lengths of the south girder, using Section 1 as the cross section, M_n = 9468k-in, when C_{b1} = 1.67 is used, and M_n = 9920k-in when C_{b2} = 1.75 is used. With Section 2 as the cross section, M_n = 10200k-in, when C_{b1} = 1.67 is used, and M_n = 10690k-in when C_{b2} = 1.75 is used. The above results are summarized in Table 3.

Table 1. Tension coupons test results.

	Yield Stress (ksi)	Ultimate Stress (ksi)	Yield Stress to Ultimate Stress Ratio
Top Flange	83.5 (576MPa)	99.2 (684MPa)	0.84
Bottom Flange	84.2 (581MPa)	95.5 (658MPa)	0.88

Table 2. Rotational stiffness parameters and effective length factors.

Girder	L_{b1} (in)	L_{b2} (in)	L_{b3} (in)	I_{yc}/I_{yf}	Ψ_1	Ψ_2	K_b for Unbraced Length	
							Inner	Outer
North	285.9	217.0	286.3	1.043	0.633	0.633	0.716	0.839
South	285.9	217.0	286.0	1.046	0.635	0.635	0.716	0.839

Table 3. Calculated lateral-torsional buckling resistance of test specimen.

Girder	Moment from Lateral-Torsional Buckling Formulas with K_b (kip-in)				
	Inner Unbraced Length	Outer Unbraced Length (Section 1)		Outer Unbraced Length (Section 2)	
	$C_b = 1$	$C_{b1} = 1.67$	$C_{b2} = 1.75$	$C_{b1} = 1.67$	$C_{b2} = 1.75$
North	11110	9424	9884	10160	10640
South	10870	9468	9920	10200	10690

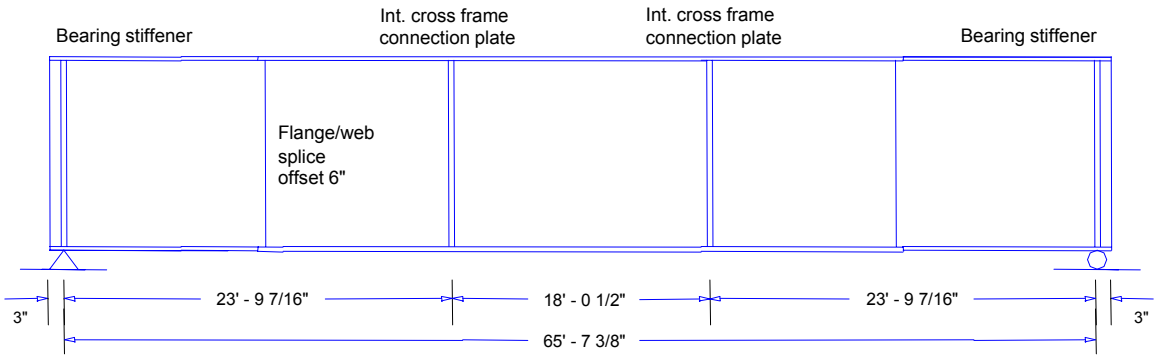

(a) Test Specimen Girder Elevation

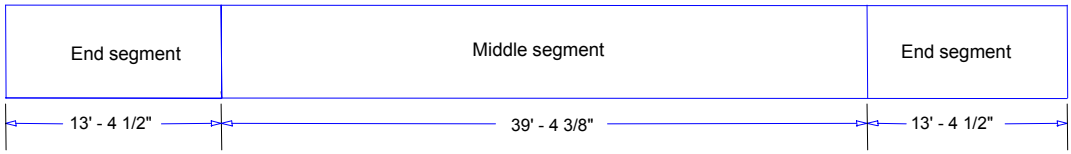

(b) Flange shop splices

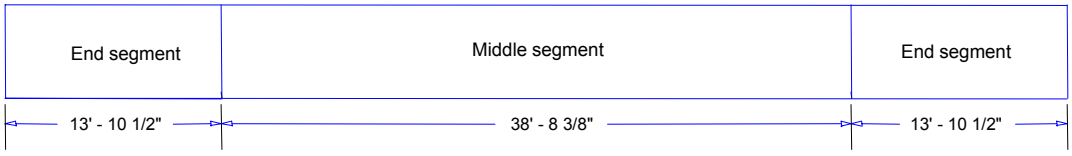

(c) Web shop splices

Figure 5. Test specimen girders.

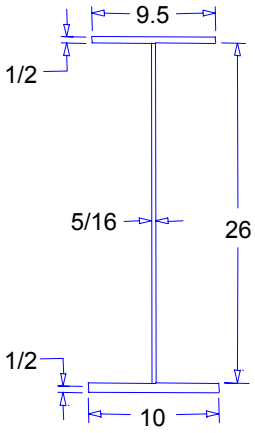

(a) End segment - Section 1

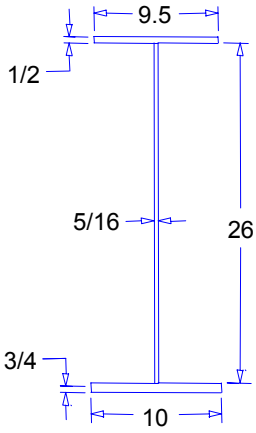

(b) Middle segment - Section 2

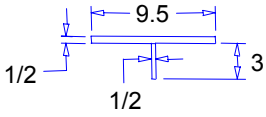

(c) FRRB

Note: Dimensions are in inches

Figure 6. Test specimen girder and FRRB nominal cross section dimensions.

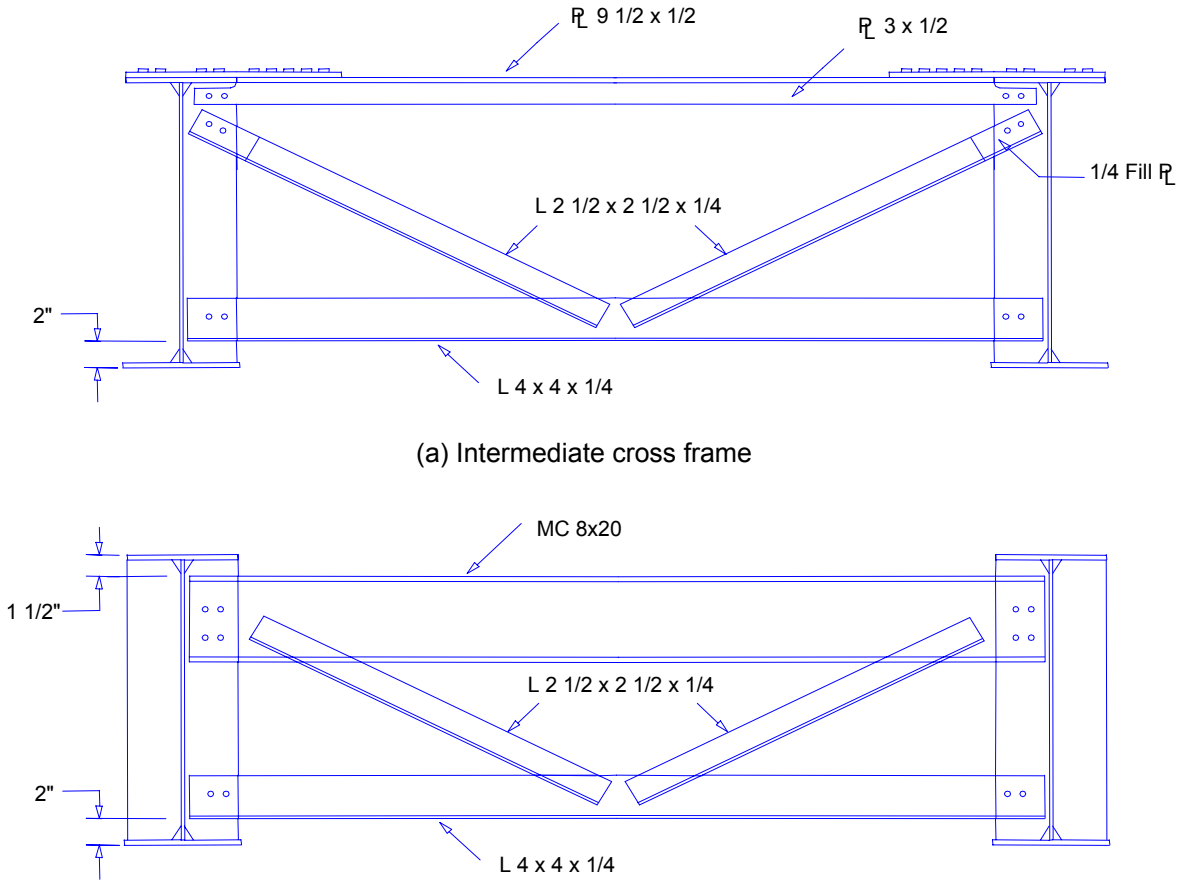

Figure 7. Test specimen cross frames.

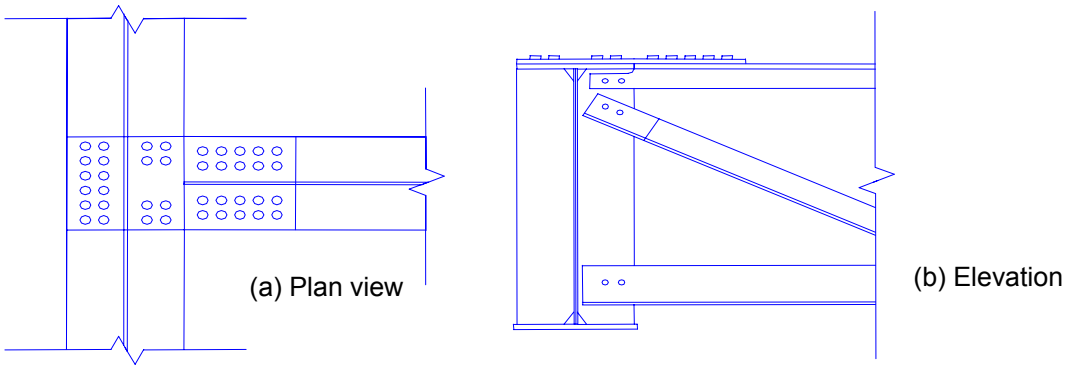

Figure 8. FRRB connection details.

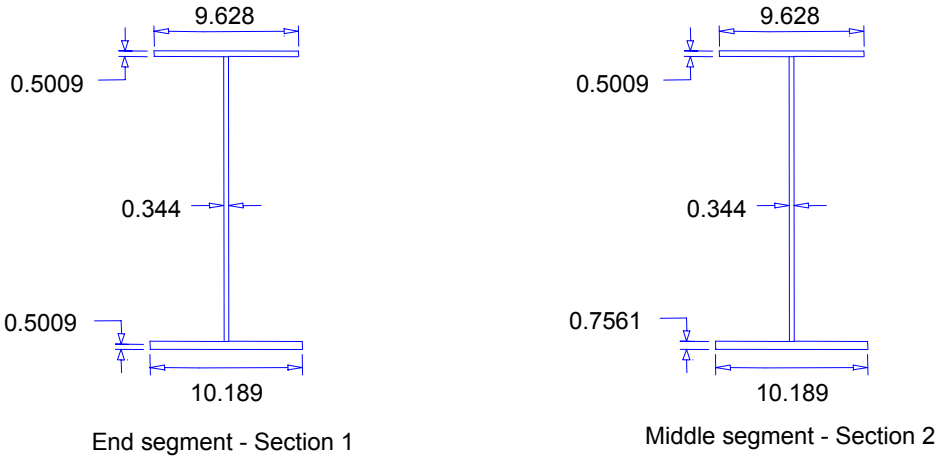

(a) North girder

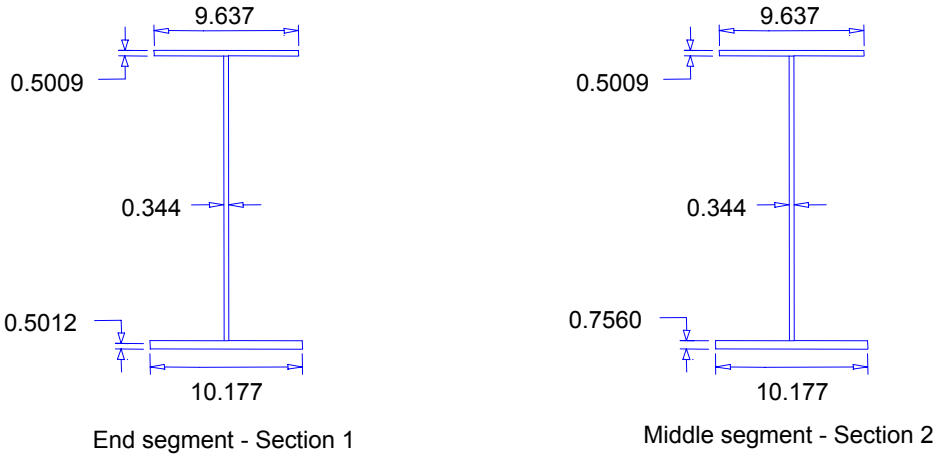

(b) South girder

Note: Dimensions are in inches

Figure 9. As-built test specimen girder cross section dimensions.

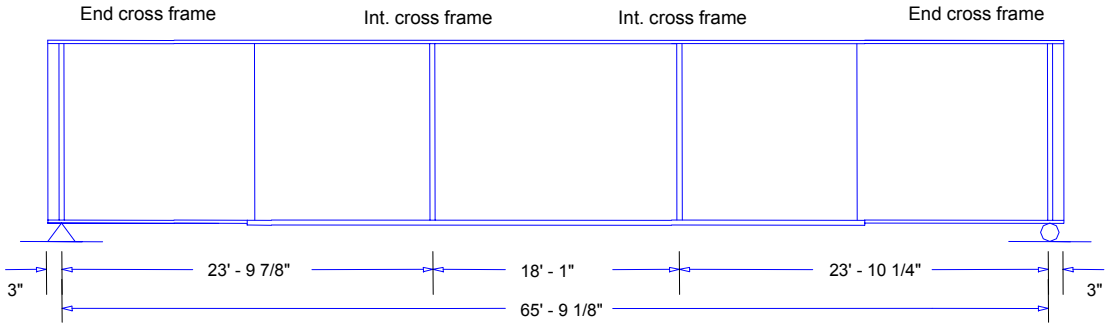

(a) North girder

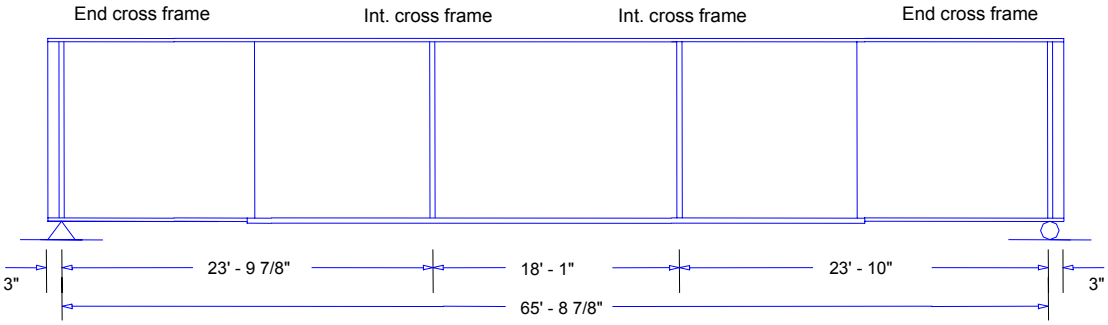

(b) South girder

Figure 10. As-built test specimen girder dimensions.

4. Test Set-Up, Instrumentation, and Procedure

4.1. Introduction

The test specimen described in Section 3 was tested to failure in lateral-torsional buckling. This section presents the test set-up, instrumentation, and procedure.

4.2. Test Set-Up

The test was conducted in Fritz Laboratory at Lehigh University. The test specimen was oriented longitudinally in the east-west direction of the lab. It was supported on two steel pedestals 39in high and 108in wide. At the bearings, each girder of the test specimen rested on a roller 6in in diameter and 10in long made of hardened steel with a nominal yield stress of 100ksi. Copper shims were placed between the roller and the girder bottom flange to help provide uniform bearing. Figure 11(a) shows a cross section of the test specimen at the end cross frame.

Figure 11(b) shows a cross section of the test specimen at the intermediate cross frame where the load was applied. Each girder of the test specimen was loaded in four-point bending with hydraulic actuators applying loads at two points on each girder (see Figure 12). In theory, this four-point loading produces a constant moment region between the intermediate cross frames and a linearly varying moment between the end and intermediate cross frames. Four hydraulic actuators with a 12in stroke were used to simultaneously apply load to both girders. One hydraulic actuator was bolted to the girder bottom flange at the location of each intermediate cross frame connection plate. Each actuator had a top and bottom clevis to allow the girders to rotate freely at the load points (see Figure 12). The clevis at the bottom of the actuator was pin connected to a steel tab, which was welded to a plate that was anchored to the laboratory floor using the floor tie-downs. Figure 13 shows photos of the test set-up.

The nominal hydraulic pressure in each actuator was the same, and each actuator had the same dimensions so it was assumed that the same load was applied at each load point by the actuators. The applied load was measured using two pressure transducers called PT1 and PT2. Four load cells were used to measure the reactions at the bearings (Figure 11(a)). The hydraulic pressure was generated by a pump. A manifold connected to the pump by a pressure line and a return line had four individual pressure lines and return lines to distribute pressure to the four actuators (see Figure 14). Pressure transducer PT1 was located at the hydraulic actuator at the west intermediate cross frame of the north girder (Figure 15) and pressure transducer PT2 was located in the pressure line between the hydraulic pump and the manifold. The two pressure transducers allowed losses in the hoses to be measured, but no significant difference in pressure measurement at the two locations was observed during the test.

4.3. Instrumentation

Instrumentation was placed on the test specimen to measure the reactions, vertical deflection, lateral deflection of the top and bottom flanges, strains in the girder and

FRRB flanges, and girder end rotations. Instrumentation was placed symmetrically on the test girders.

The locations of the load cells, displacement transducers, and rotation meters on each test girder are shown in Figure 16. A load cell was placed at each bearing. Vertical deflection was measured using vertical displacement transducers attached to the girder bottom flange at the girder midspan and at 21ft east and west of the girder midspan. Lateral deflection of the girder top and bottom flanges was recorded using horizontal displacement transducers at the same locations as the vertical displacement transducers. The lateral displacement transducers were attached to the exterior edges of the girder flanges. Rotation meters were placed on the bearing stiffeners.

Strain gages were placed on the girder top and bottom flange and the FRRB flange to measure the longitudinal strains. Strain gages located along the two longitudinal edges of the top surface and bottom surface of the top flange of girders were used to measure the lateral bending strains of the top flange. Strain gages located at the centerline of the top and bottom flanges were used to measure the strains due to the primary bending.

Figure 17 shows that seven cross sections were chosen to locate the strain gages on each girder. Two types of strain gage sets were used for the seven sections. One strain gage set used a total of five strain gages on the cross section, and is called the 5-strain-gage section. Four of the strain gages were located along the longitudinal edges of the top and bottom surface of the top flange, and one of the strain gages was on the centerline of the bottom surface of the bottom flange. The second strain gage set used a total of four strain gages on the cross section and is called the 4-strain-gage section. Three of the four gages were on the top surface of the top flange and one of the four gages was on the centerline of the bottom surface of the bottom flange.

Three cross sections on each FRRB were chosen for locating the strain gages. Two strain gages were placed along the two longitudinal edges of the flange of the FRRBs at each section (see Figure 17).

4.4. Test Procedure

The test specimen was loaded in two phases: (1) two elastic cycles up to 17kips, and (2) load to failure. The elastic loading cycles were used to align and properly seat the specimen, and check the instrumentation. The hydraulic actuators applied load at a rate of approximately 1kip per minute. The loading rate was approximately equal to a displacement rate of 0.25in per minute. This loading rate remained constant until failure. Throughout the elastic loading cycles, and the loading to failure, data from instrumentation was recorded by an automated data acquisition system.

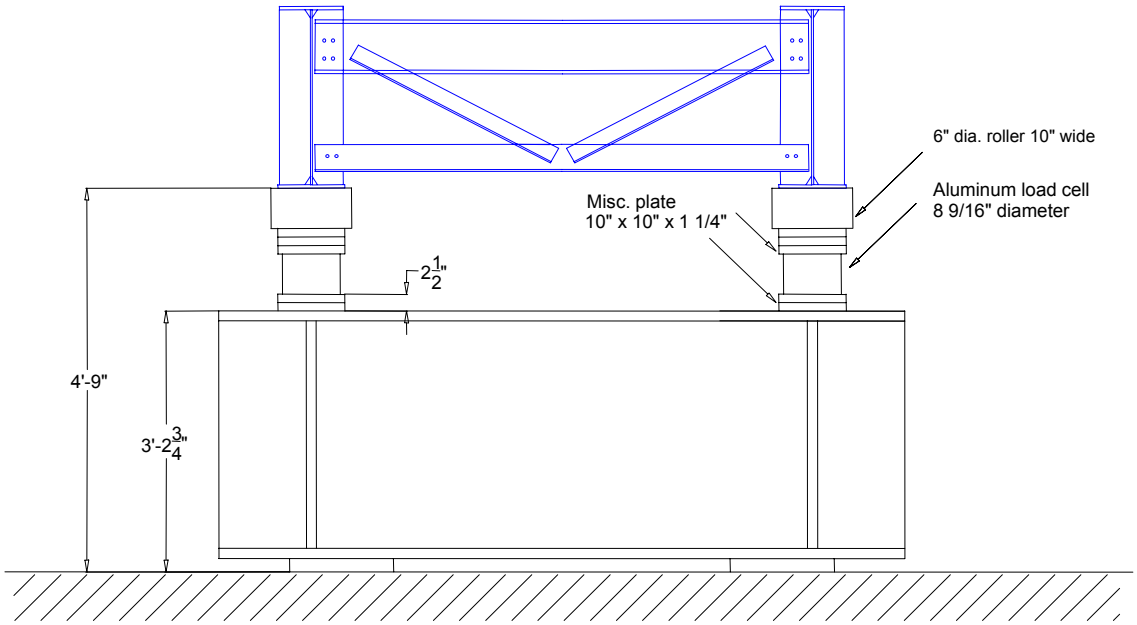

(a) Test set-up end view

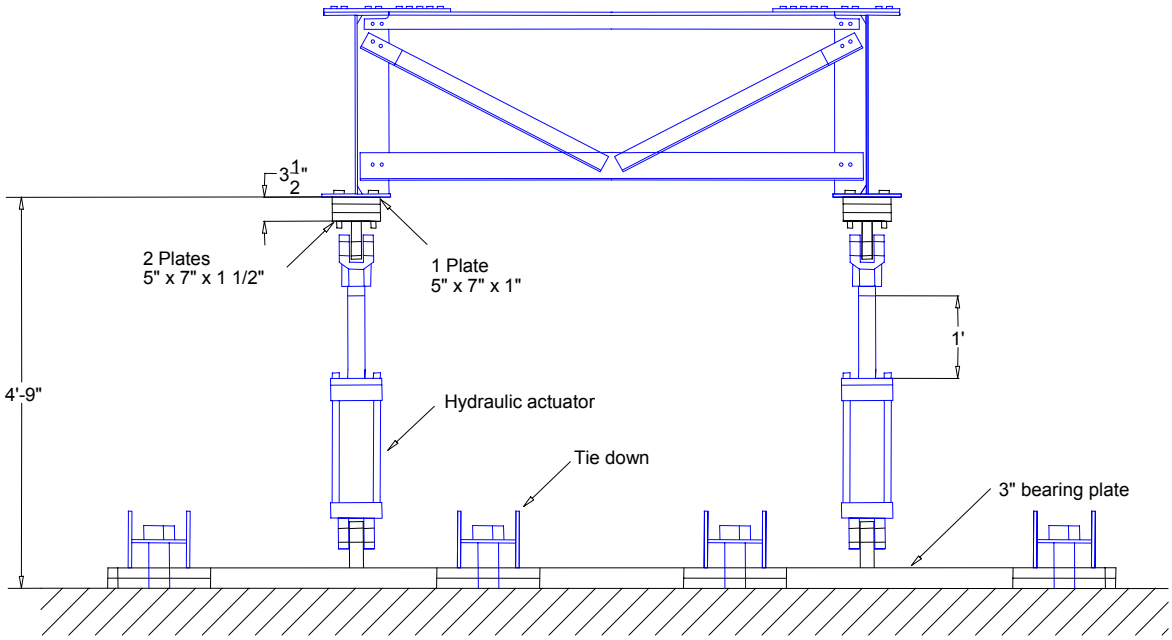

(b) Cross section view near intermediate cross frame

Figure 11. Test set-up.

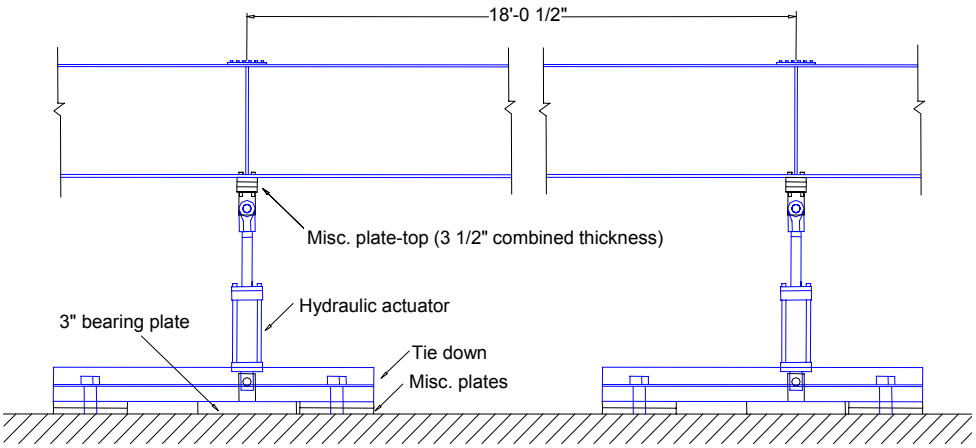

Figure 12. Test set-up elevation view near intermediate cross frames.

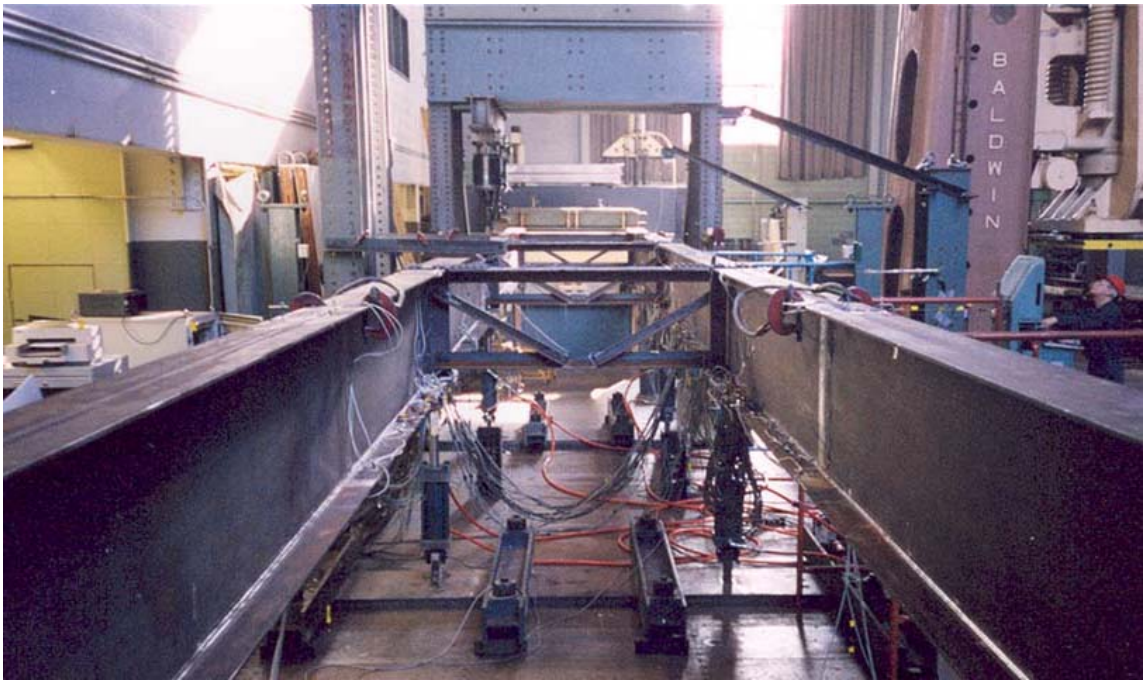

Figure 13. Photograph of test set-up.

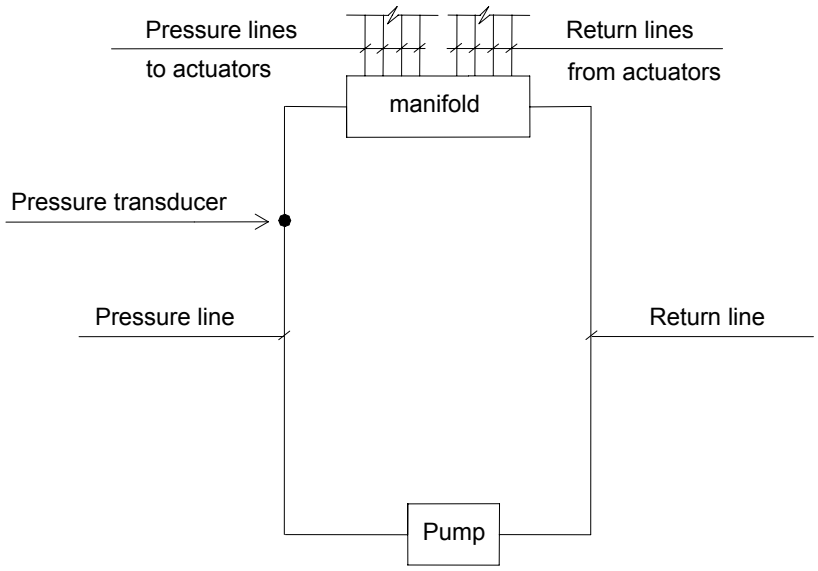

Figure 14. Schematic of hydraulic pump and manifold system.

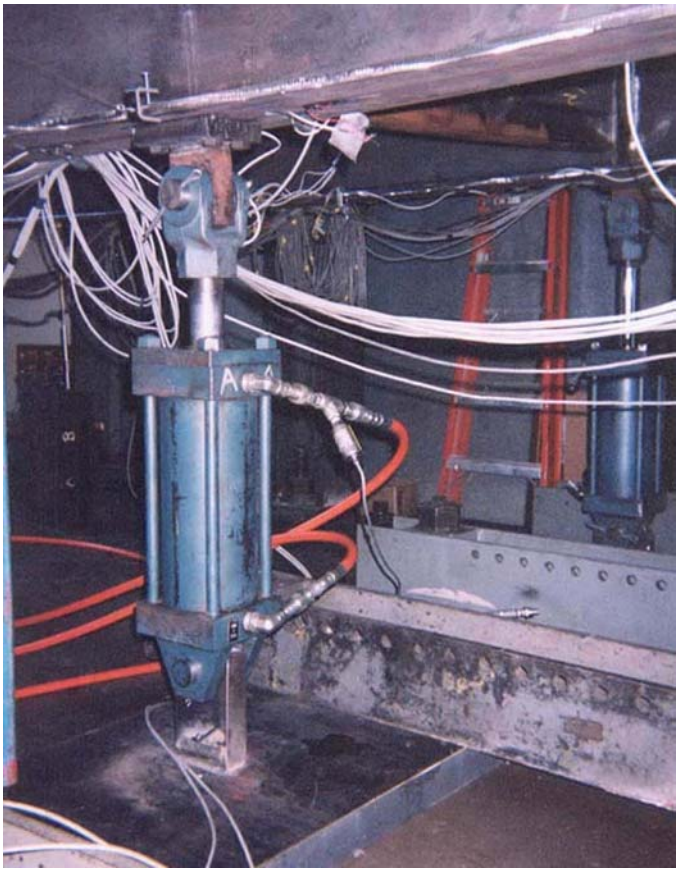

Figure 15. Photograph of hydraulic actuator with pressure transducer PT1.

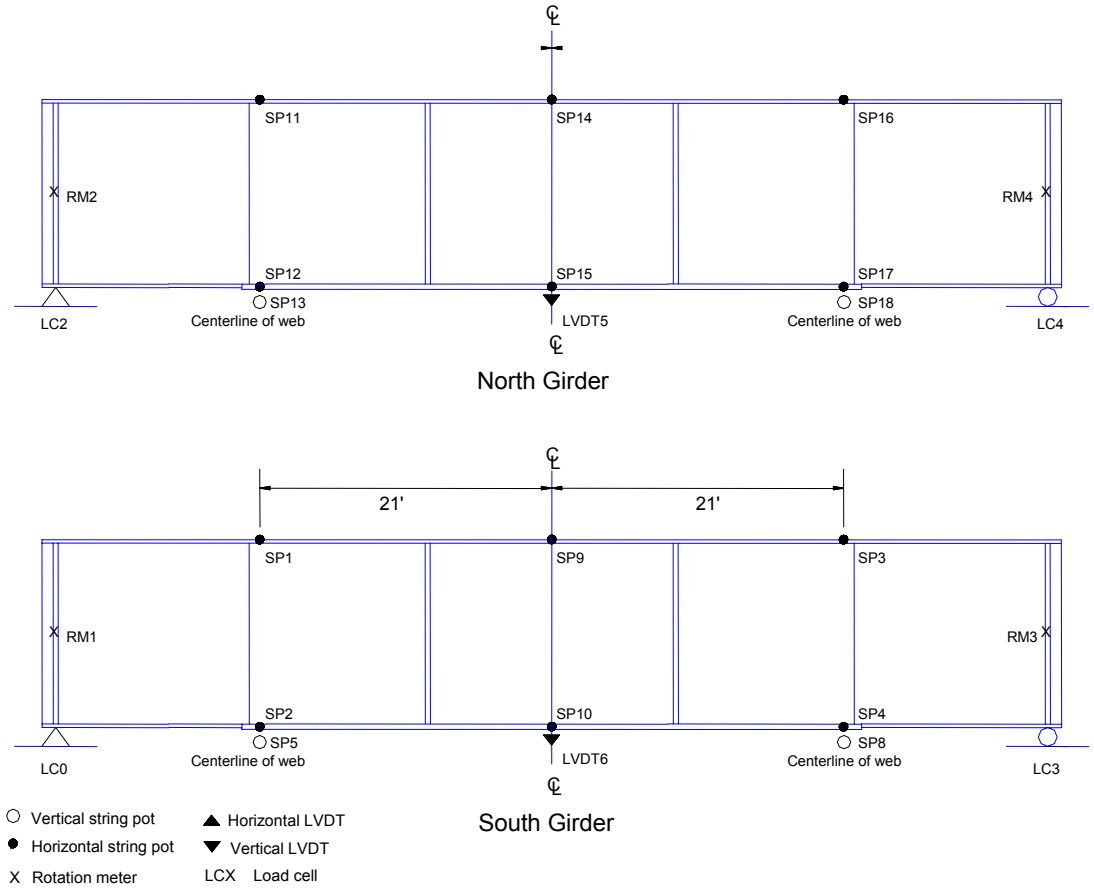

Figure 16. Deflection, rotation, and reaction instrumentation.

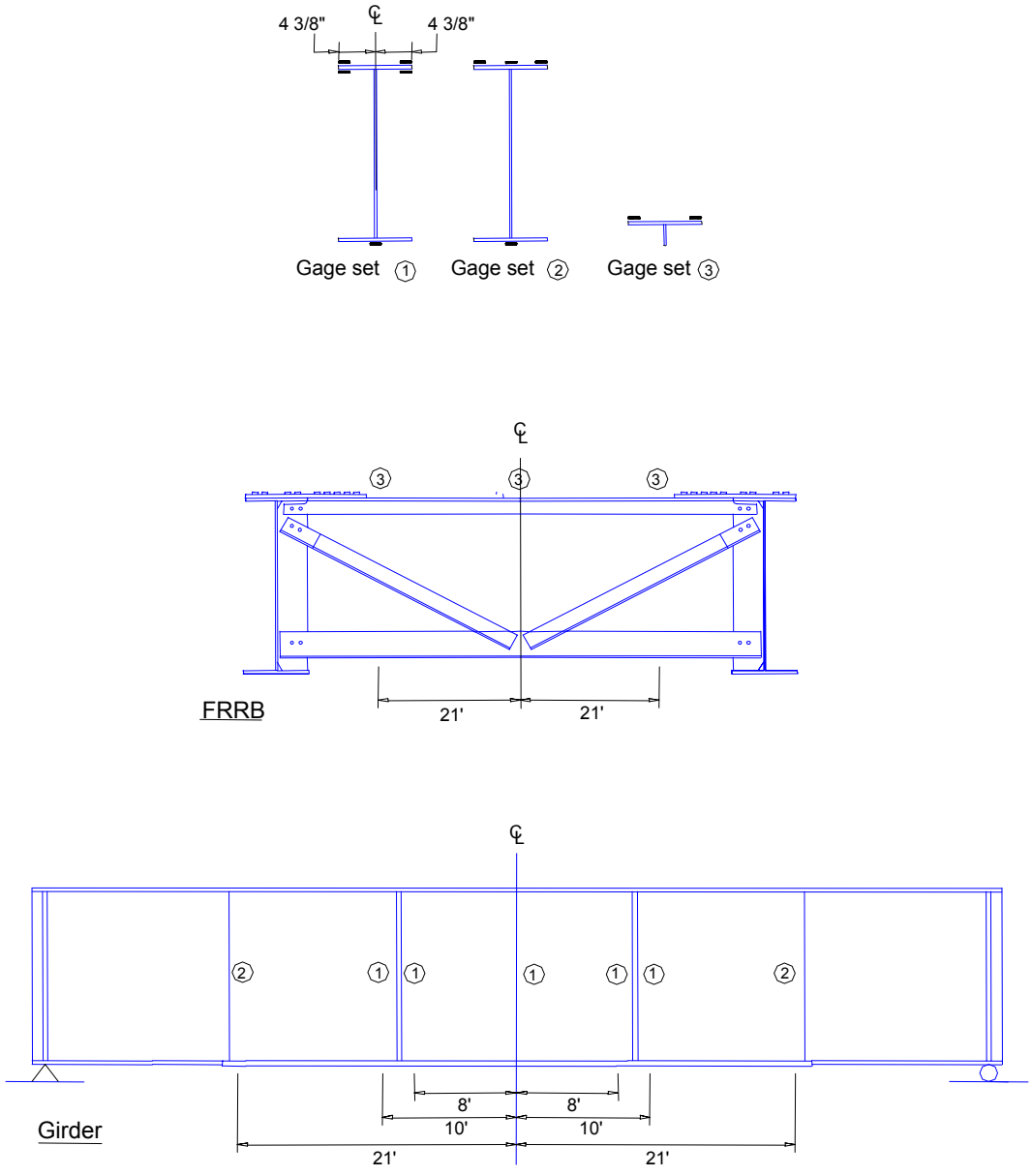

Figure 17. Strain gage sets.

5. Test Results

5.1. Introduction

This section summarizes the results of the failure test of the specimen described in Section 4. Results for the applied load, I-girder flange and FRRB lateral curvature, I-girder lateral deflection, and moment capacity are presented. The test results are compared to the calculated results for the test specimen, and the behavior of the test specimen is compared with the behavior assumed by the analysis method.

5.2. Applied Load

As discussed in Section 4, the test specimen was loaded using hydraulic actuators. The load was controlled by the pressure in the hydraulic lines, which was measured by pressure transducers. A pretest calibration was conducted to relate the pressure in the hydraulic actuators to the corresponding load applied by the actuator. As shown in Figure 18, one of the actuators was placed in a universal test machine and pressure was applied in the actuator and measured. The load measurements from the test machine were plotted versus the measured pressure, and a regression was used to determine a calibration factor between the pressure measured by the pressure transducers and the load developed by the actuators. Pretest calibrations of the load cells used at the bearings of the test specimen were also conducted.

Despite these pretest calibrations, discrepancies in loading and unloading of the test specimen were observed. Figure 19 shows the load determined from the calibrated pressure transducer, PT1, versus the reaction measured by the calibrated load cells at the bearings. The load, shown on the vertical axis, is assumed to be applied by each of the four actuators in the test set-up shown in Figures 12 and 13. A simple static analysis suggests that each reaction should equal the load in each actuator (*i.e.*, as determined from PT1). However, differences exist between the load from the pressure transducer, PT1, and the reactions for the loading branch of the test. These differences are attributed to redistribution of the reactions by the end cross frames due to differences in the seating of the I-girders at the bearings. Data presented later shows that the girder shears at the bearings were similar to each other. Also, the sum of the measured reactions is quite close to the applied load from PT1 multiplied by 4.

Significant differences between the load from PT1 and the reactions are observed also during unloading due to friction within the actuators. The friction force influences the relationship between the applied load and pressure because it is opposite to the direction of the actuator movement. The friction force changes direction when the actuator movement changes direction, as follows.

During the loading phase of the test, the load applied to the test specimen produces downward deflection of each girder. The friction force opposes the downward movement of the actuator piston and opposes the force generated by the pressure, thus reducing the load applied to the girder (see Figure 20(a)). This effect was taken into account during the pretest calibration relating the pressure in the hydraulic actuators to the applied force.

During unloading of an elastic girder, as the load decreases, the deflection of the girder decreases. In this case, the friction force opposes the upward movement of the piston and is in a direction opposite to that in the loading phase. The friction force thus increases the load applied to the girder (see Figure 20(b)).

If the girder is failing during unloading, as the load on the girder decreases, the deflection of the girder continues in the downward direction. Thus, the friction force still opposes the force generated by the pressure, and reduces the load applied to the girder (see Figure 20(c)).

The relationships between the applied load and pressure are summarized as follows:

- Loading of an I-girder:
  applied load = pressure × piston area – friction (18)
- Unloading of an elastic I-girder:
  applied load = pressure × piston area + friction (19)
- Unloading of a failing I-girder:
  applied load = pressure × piston area – friction (20)

Using the above formulas to analyze Figure 19, we observe that the south girder, which is supported by load cell LC0 and load cell LC3, is unloading elastically. For the plots of load (from PT1) versus reaction from load cell LC0 and load cell LC3, the unloading path is different from the loading path, which suggests that the relationship between applied load and pressure for unloading phase is different from the relationship for the loading phase. The friction force increases the applied load during the elastic unloading as the deflection direction of the south girder changes from downward to upward. This increase in applied load is seen in the figure as an apparent (nearly vertical) *decrease* in load obtained from the pressure transducer PT1, because the pressure drops while the reaction measured by load cell LC0 and load cell LC3 does not drop, because of the increase in applied load from the friction force. For this case, the applied load during unloading is determined by Equation 19.

From the plots of load (from PT1) versus the reaction from load cell LC2 and load cell LC4, we observe that the north girder, which is supported by load cell LC2 and load cell LC4, is failing during unloading. The unloading path of north girder is the same as the loading path of north girder until the test was stopped at the point identified in the figure with the **X** symbol. The friction force decreases the applied load during unloading, and the relationship between applied load and pressure is the same for the unloading phase (Equation 20) and the loading phase (Equation 18) of the test.

During the test, visual observations suggested that that north girder failed and the south girder did not. Figure 21 shows a photograph of the north girder when the load is near the peak load. The figure shows the beginning of significant lateral deflection of the north girder compression flange. Figure 22 shows a photo of the north girder after the peak load is reached. Significant lateral deflections of the compression flange are observed.

The failure of the north girder is further confirmed by the vertical deflections the midspan of test girders. Figure 23(b) shows the vertical deflection of the south girder returns toward zero during unloading. The nearly vertical drop in the load obtained from the pressure transducer PT1 observed just after the peak load is a result of the friction in the actuators. Figure 23(a) shows the vertical deflection of the north girder kept increasing

during unloading until test was stopped (at the **X** symbol). After the test was stopped, there is a nearly vertical drop in the load obtained from the pressure transducer PT1, because the deflection direction of the north girder changes from downward to upward and the friction force decreases the applied load during this elastic unloading of the north girder after the test was stopped.

5.3. Girder Top Flange Lateral Curvature

The lateral curvature of the top flange of the test girders was obtained from the strain gage data. The difference between the strain from a north edge strain gage and the strain from a south edge strain gage was divided by the distance between the two strain gages, as follows:

$$\varphi = \frac{\varepsilon_{north} - \varepsilon_{south}}{b} \tag{21}$$

where,

φ is the lateral curvature,
ε_{north} is the strain at the north edge of the flange,
ε_{south} is the strain at the south edge of the flange,
b is the distance between the two strain gages.

When the curvature is positive, the north edge strain gages are in tension and south edge strain gages are in compression, and the center of curvature is to the south. The curvature is calculated from strains with units of microstrain, and the unit of curvature is 10^{-6}/in.

Figures 24(a) and 24(b) show flange lateral curvature results at the sections with strain gages along the north girder and south girder respectively. The figures show the lateral curvature of the top flange at different load levels. For example, the 25% data indicates the curvature at an applied load of 25% of the peak load.

5.4. FRRB Lateral Curvature

Figure 25 shows the FRRB lateral curvatures calculated from strain gage data using an equation similar to Equation 21. Figure 24(b) shows that the west FRRB curvature is nearly the linear but not constant. The lateral curvature, and therefore the lateral bending moment at the south end of the west FRRB is far smaller than that at the north end. Figure 25(a) shows that the east FRRB initially develops constant curvature, and therefore constant bending moment, up to 75% of the peak load. However, at the peak load, the bending appears to be nonlinear over the FRRB length, which is unreasonable since lateral forces are not applied within the FRRB length. Error in the strain gage data appears to be the source of this unreasonable result.

In Section 2 of the report, Figure 4(b) suggests that the curvature and corresponding lateral bending moment along the length of an FRRB should be constant. This figure is based on the assumption that the two girders braced by an FRRB behave similarly, and that the lateral curvatures and deflections in the two unbraced lengths adjacent to the FRRB are in opposite directions. The corresponding lateral deflected shape of each girder has inflection points near the connection with the FRRBs (Figure 4(b)). However, Figure 24(b) (and, later, Figure 26(b)) show that the curvatures (and, later, the

deflections) in the two unbraced lengths of the south girder that are adjacent to the west FRRB are in the same direction. The center of curvature in these two unbraced lengths near the west FRRB is to the north (negative) on both sides of the FRRB. Later, it is shown that this result for the top flange of the south girder is due to its initial lateral deflection (out-of-straightness). The resulting deflected shape of the south girder does not significantly rotate the south end of the west FRRB and this leads to a small lateral bending moment at south end of the west FRRB (as shown by the curvature given in Figure 25(b)). In other words, the south end of the west FRRB does not need to develop a lateral bending moment to restrain the south girder. However, at the north end of the west FRRB, the north girder compression flange lateral curvatures are as expected from Figure 4(b) (see Figure 24(a) and Figure 22). Therefore, the north end of the west FRRB develops a lateral bending moment to restrain the north girder, as shown in Figure 25(b).

5.5. Girder Top Flange Lateral Deflection

Figure 26 shows the lateral deflection of the top flange of test girders at different load levels during the test. These deflections do not include the initial lateral deflection (out-of-straightness) of the girder top flanges, which was measured before the tests. The initial out-of-straightness was added to the lateral deflections of the top flanges during the test to determine the total lateral deflection. Figure 27 shows the initial out-of-straightness of the top flanges of the test girders, and Figure 28 shows the total lateral deflection of the top flanges of the test girders.

As expected, the lateral deflections of the top (compression) flanges of the test girders are substantially influenced by the initial out-of-straightness. It is seen from Figure 28 that the deflected shape of the south girder top flange during the test is not as suggested by Figure 4(b) due to the initial out-of-straightness of the flanges (see Figure 27(b)). The initial out-of-straightness of the south girder is in the same direction in the inner unbraced length and the west outer unbraced length, and the magnitude of the initial out-of-straightness is larger than the additional lateral deflections during the test (Figure 26(b)). As a result the lateral deflected shape of south girder is significantly different from that suggested in Figure 4(b). The inner unbraced length and the west outer unbraced length deflect in the same direction during the test, and the inflection points near the connection of south girder to the west FRRB do not form as expected.

The initial out-of-straightness of the top flange of the north girder is smaller than that of the south girder, and the total lateral deflected shape of north girder top flange (Figure 28(b)) is consistent with that Figure 4(b). Thus, the results show that the initial out-of-straightness of the top flange significantly influences the lateral deflected shape during the test. The lateral deflected shape shown in Figure 4(b) produces the lowest lateral buckling mode of the combined system (two girders with cross frames and FRRBs). The initial out-of-straightness of the south girder forces it into a higher buckling mode with a corresponding higher buckling load. The north girder has a total lateral deflected shape during the test similar to that of Figure 4(b), and therefore the north girder failed by lateral-torsional buckling during the test.

5.6. Moment at Lateral-Torsional Buckling

Three methods are used to calculate the lateral-torsional buckling moment capacity from the test results. The moment capacity is defined as the major principle axis bending moment at the peak load within the theoretical region of constant bending moment between the load points of the test girders.

Method 1
The moment at each section with attached strain gages is calculated from the bending strain at the top and bottom flanges using beam theory as follows:

$$M = \frac{\varepsilon_{top\_flange} - \varepsilon_{bottom\_flange}}{Y_\varepsilon} EI \tag{22}$$

where,

ε_{top_flange} is the strain of the top flange due to primary bending,
$\varepsilon_{bottom\_flange}$ is the strain of the bottom flange due to primary bending,
EI is the bending stiffness about the major principle axis, x, of the girder section,
Y_ε is the distance between the top and bottom flange primary bending strains.

For the 5-strain-gage sections discussed in Section 4.3, ε_{top_flange} is equal to the average of the four gages on the top flange. For the 4-strain-gage sections, ε_{top_flange} is the average of the two gages on the edges of the top flange. In both cases, $\varepsilon_{bottom\_flange}$ is the strain of the bottom flange from the single gage on the bottom flange. For the 5-strain-gage sections, Y_ε is the distance from the middle surface of the top flange to the bottom surface of the bottom flange. For the 4-strain-gage sections, Y_ε is the distance from the top surface of the top flange to the bottom surface of the bottom flange. The moment diagrams of the test girders from Method 1 are shown in Figure 29.

Method 2
The results in Figure 29 are not as expected from static analysis of the test set-up and this is likely due to local flange yielding at certain locations which invalidates Equation 22. Thus, a second method based on the moment diagram obtained from Method 1 was developed. The method assumes that the bending moments in the boxes in Figure 29 are correct. These bending moments are at locations where yielding did not occur. Then these moments are used to determine the shear forces at the bearings according to equations of statics. From the shear forces at the two ends, the moments at the other sections of the girders are obtained from statics knowing that the loads were applied to the girders at only the intermediate cross frame locations. The moment diagrams from Method 2 are shown in Figure 30.

Method 3
The moment is calculated assuming the peak load determined from pressure transducer PT1 is applied at all four load points of the test set-up. From statics, this peak applied load of 33.97 kips produces a constant maximum moment of 9715k-in in the regions between the load points at the intermediate cross frame locations.

The results from Method 1 are not considered accurate. The results from Method 2 and Method 3 are shown in Table 4. These results are within 3% of each other.

5.7. Comparison with Calculated Lateral-Torsional Buckling Resistance

According to the moment resistance obtained from lateral torsional buckling formulas including an effective length factor, K_b, discussed in Section 2 (see the Table 5), the inner unbraced lengths of the test girders have higher moment capacities than the outer unbraced lengths. Also, the outer unbraced length of the north girder has a lower moment capacity than that of the south girder. So the outer unbraced lengths of the north girder should be expected to fail in lateral-torsional buckling first.

The moment capacity of the test girders obtained from the test (Table 4) can be compared with these calculated results. The calculated moment capacity of the outer unbraced length of the north girder is in the range of 9424kip-in to 10160kip-in for C_{b1} = 1.67 (see Table 5). The average of these two moments is 9792kip-in. The moment capacity of the north girder (Table 4) from the test ranges from 9459kip-in and 9751kip-in. The average of these values is 9660kip-in. These test results are very close to the calculated results from the lateral torsional buckling formulas including K_b. The difference is 1.4%. The agreement between the test results and calculated results shows that the use of the lateral torsional buckling formulas with the effective length factor K_b is a relatively accurate way to determine the lateral-torsional buckling moment resistance of the bridge I-girders with cross frames and FRRBs.

5.8. Comparison with Behavior Assumed by Analysis Method

The top flange lateral curvature and lateral deflection data for the north girder show that when the top flange initial lateral deflection (out-of-straigntness) is favorable for lateral-torsional buckling, the behavior assumed in developing the analysis method and illustrated in Figure 4(b) is observed. In this case, the lateral-torsional bucking moment resistance obtained using the lateral torsional buckling formulas with K_b can be expected to be reasonably accurate. However, the data for the south girder shows that when the top flange initial lateral deflection (out-of-straigntness) is not favorable for lateral-torsional buckling, the behavior assumed by the analysis method will not be observed. In this case the lateral-torsional bucking moment resistance obtained using the lateral torsional buckling formulas with K_b can be expected to be less than the actual moment capacity.

Table 4. Major principle axis bending moment at load points and at midspan.

	North Girder (kip-in)			South Girder (kip-in)		
	East FRRB	Mid-Span	West FRRB	East RRB	Mid-Span	West FRRB
Method 2	9459	9605	9751	9566	9482	9398
Method 3	9715	9715	9715	9715	9715	9715

Table 5. Calculated lateral-torsional buckling resistance of test specimen.

Girder	Moment from Lateral-Torsional Buckling Formulas with K_b (kip-in)				
	Inner Unbraced Length	Outer Unbraced Length (Section 1)		Outer Unbraced Length (Section 2)	
	$C_b = 1$	$C_{b1} = 1.67$	$C_{b2} = 1.75$	$C_{b1} = 1.67$	$C_{b2} = 1.75$
North	11110	9424	9884	10160	10640
South	10870	9468	9920	10200	10690

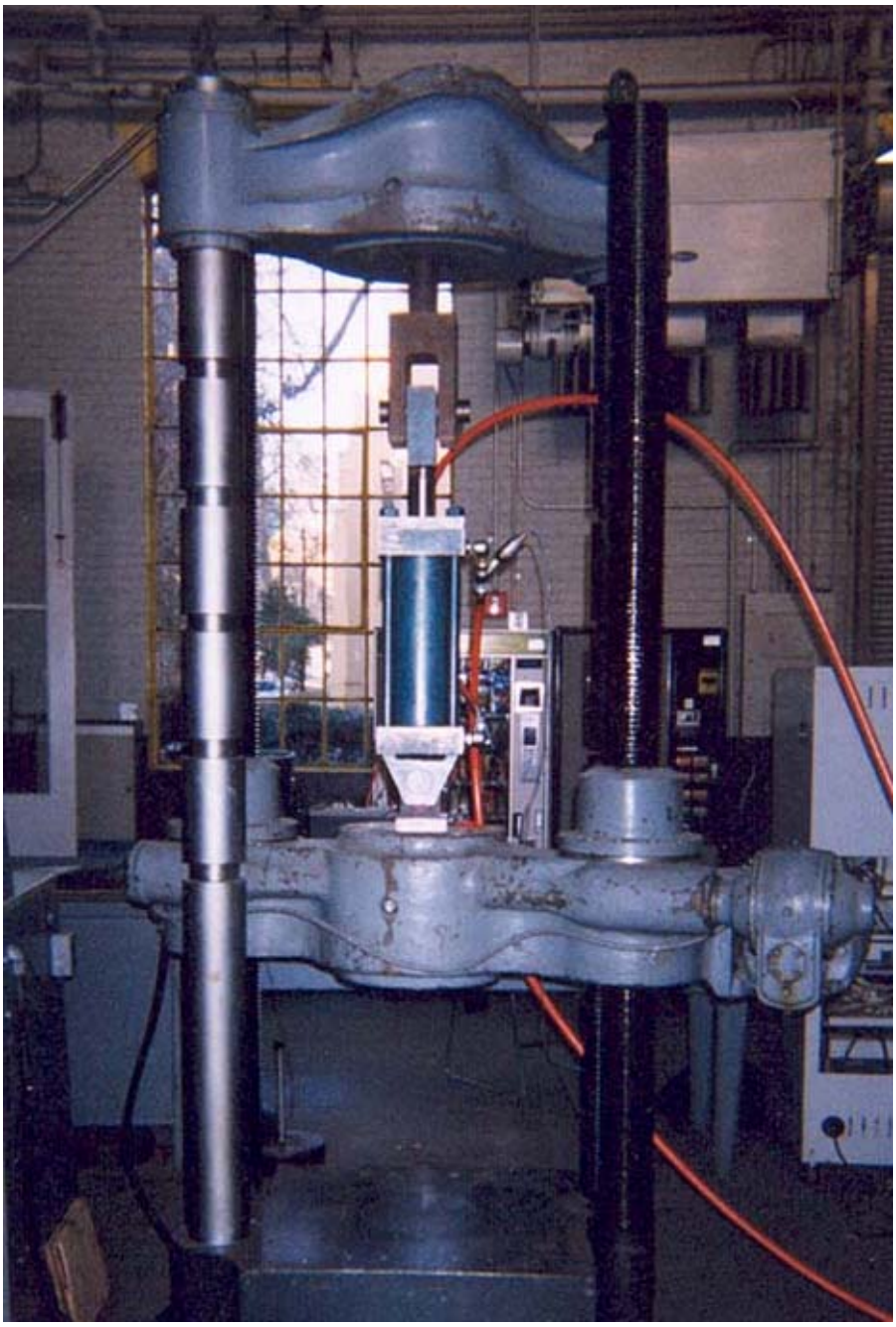

Figure 18. Photograph of actuator calibration.

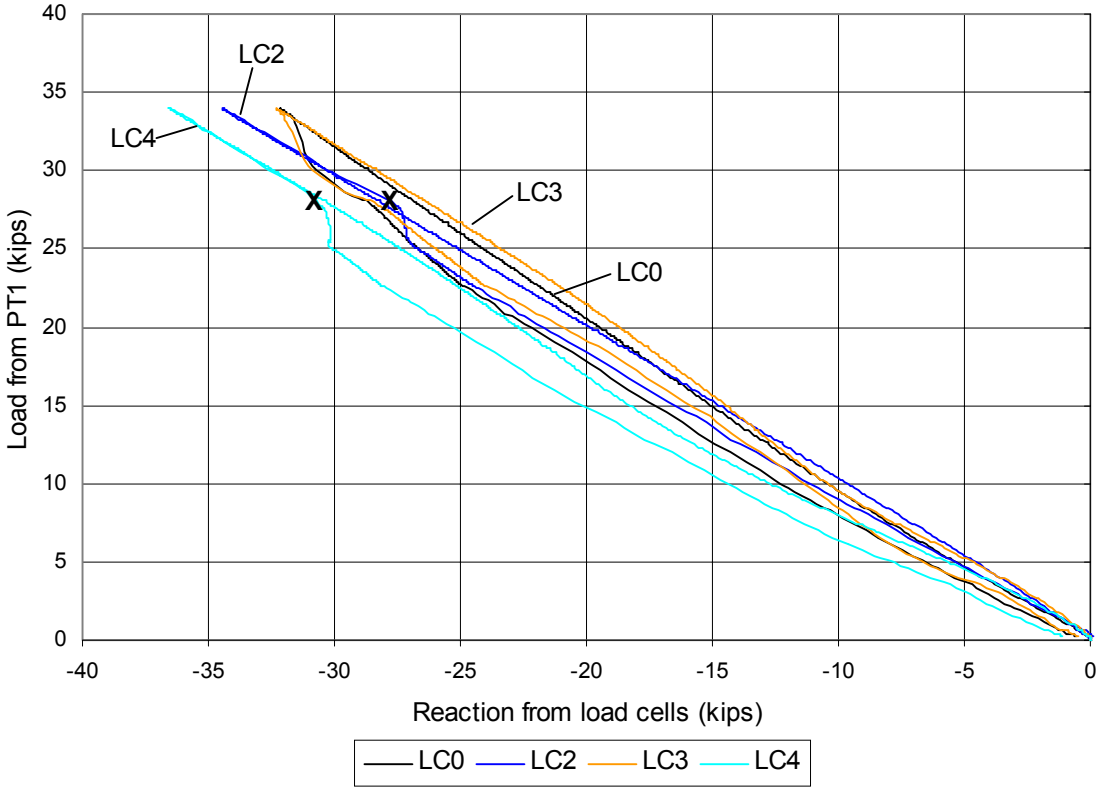

Figure 19. Load from pressure transducer versus measured reactions.

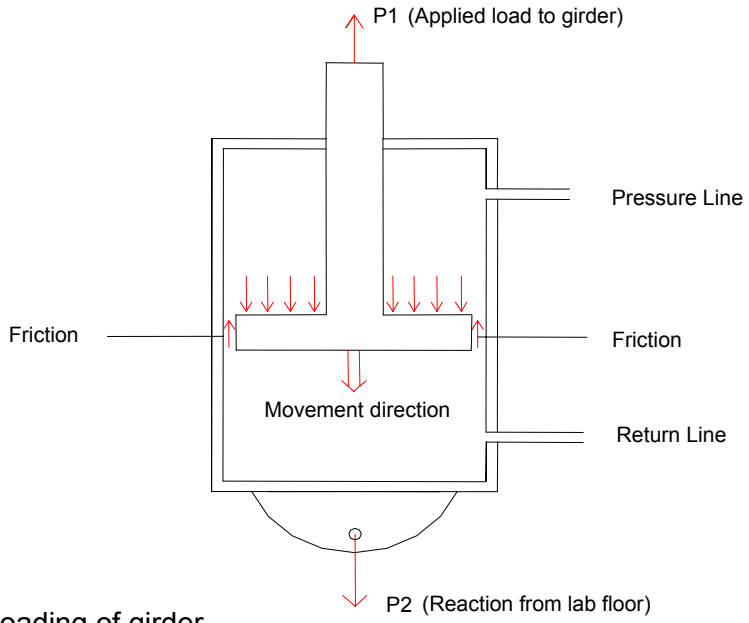

(a) Loading of girder

Figure 20. Relationship between applied load and pressure in actuator.

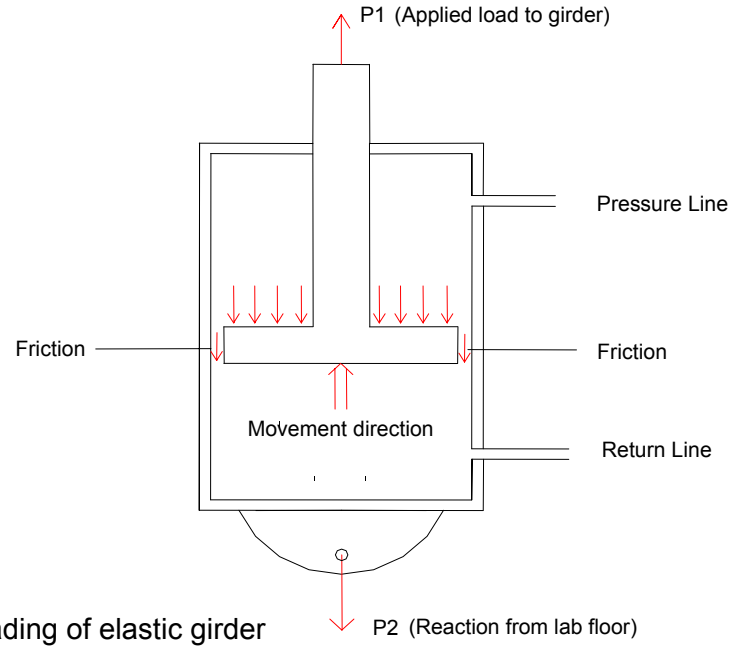

(b) Unloading of elastic girder

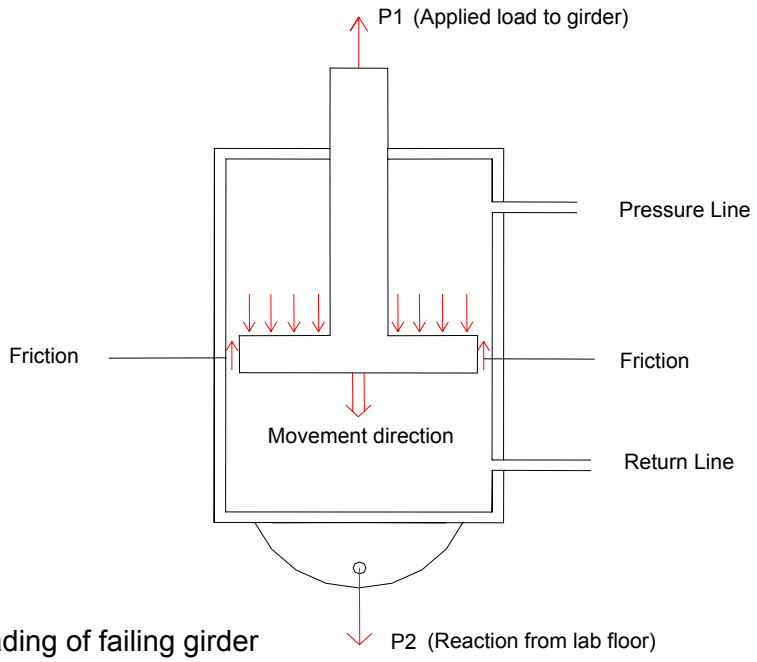

(c) Unloading of failing girder

Figure 20. Relationship between applied load and pressure in actuator (cont.).

Figure 21. Photograph of north girder at peak load.

Figure 22. Photograph of north girder after peak load.

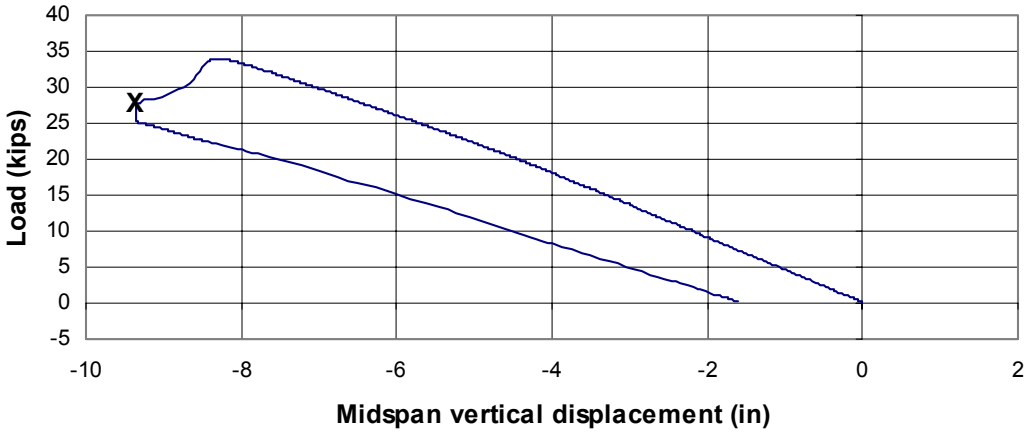

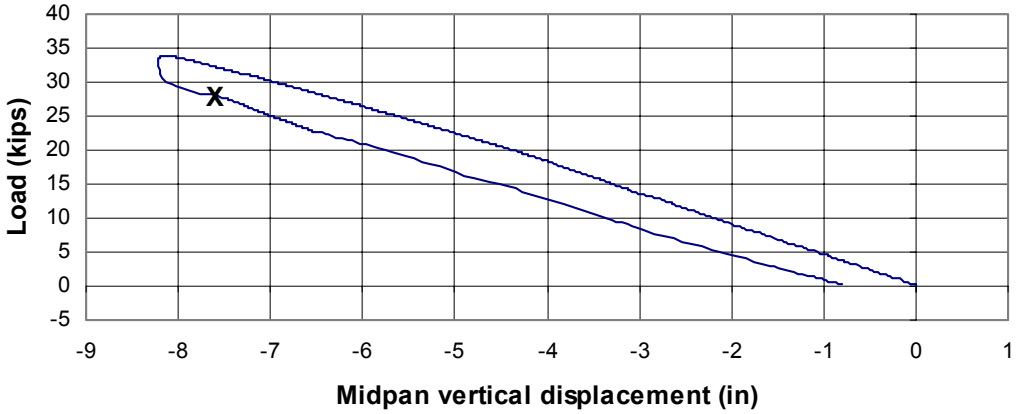

Figure 23. Load versus midspan vertical deflection.

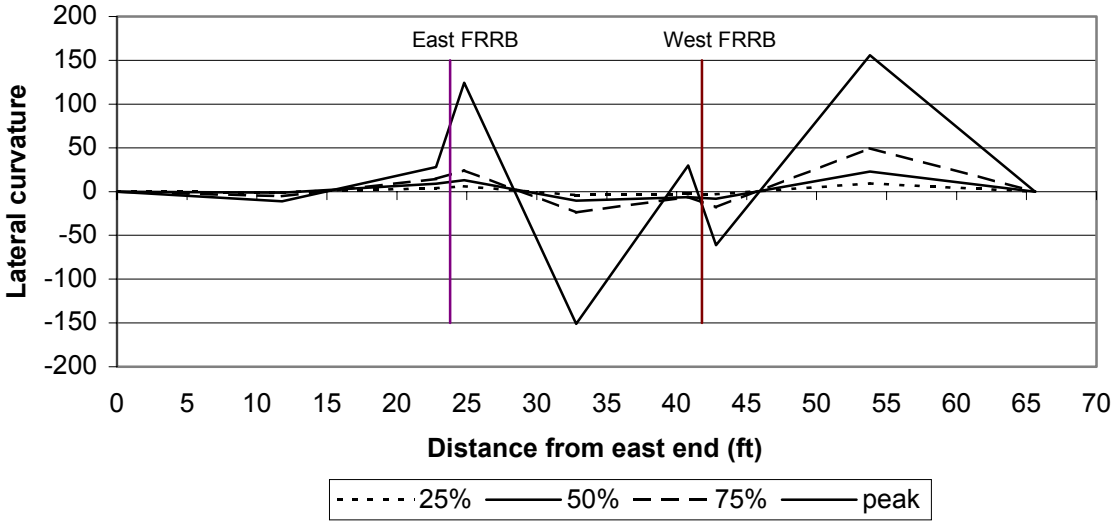

(a) North girder

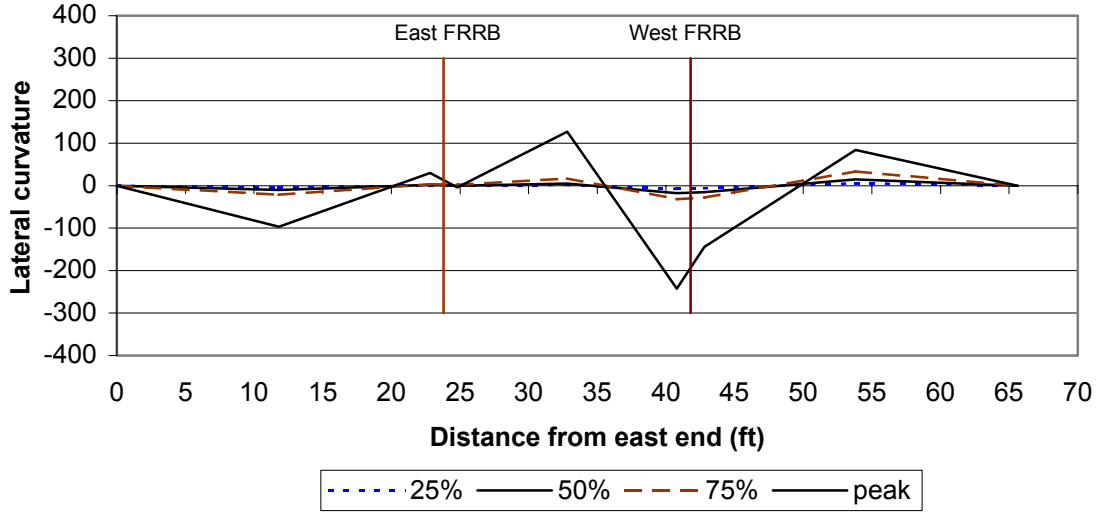

(b) South girder

Figure 24. Girder top flange lateral curvature (x10^{-6}/in) at different load levels.

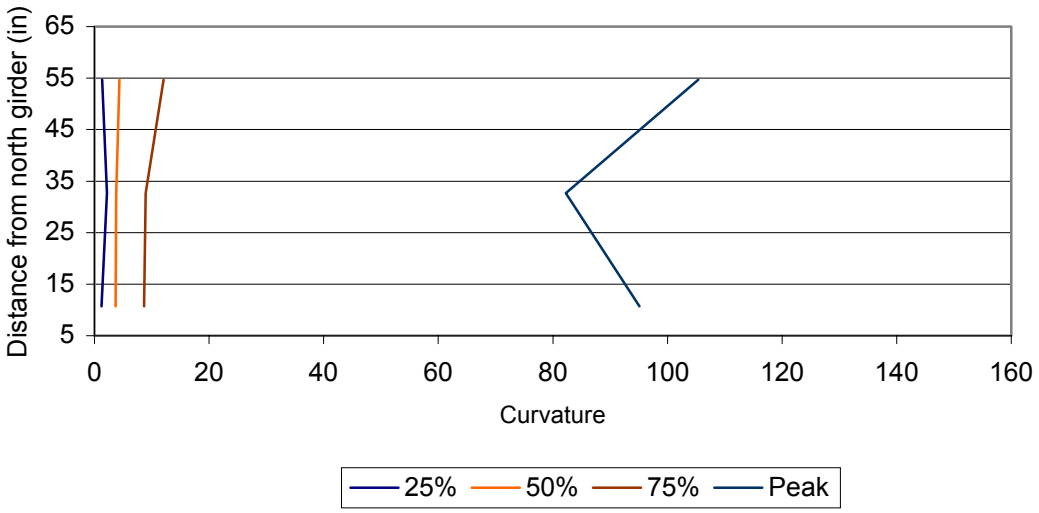

(a) East FRRB

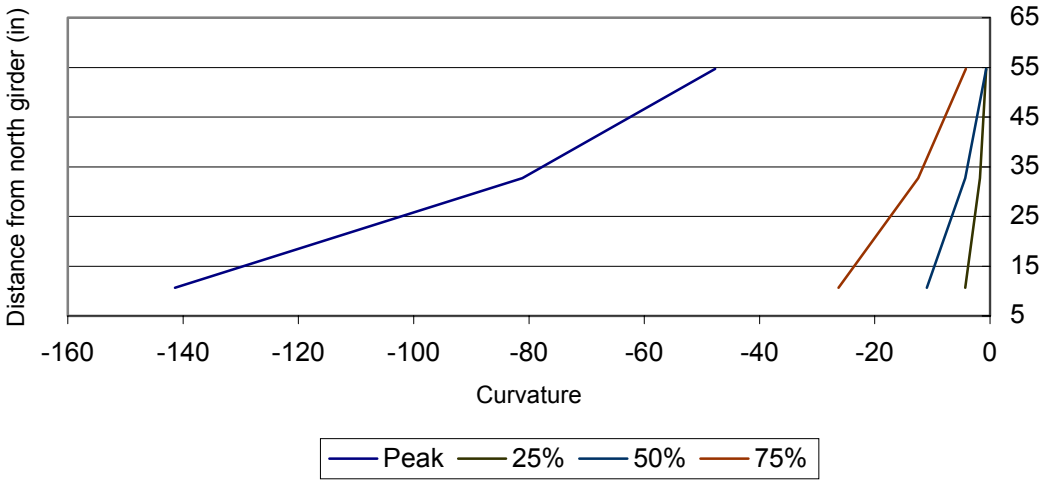

(b) West FRRB

Figure 25. FRRB lateral curvature (x10^{-6}/in) at different load levels.

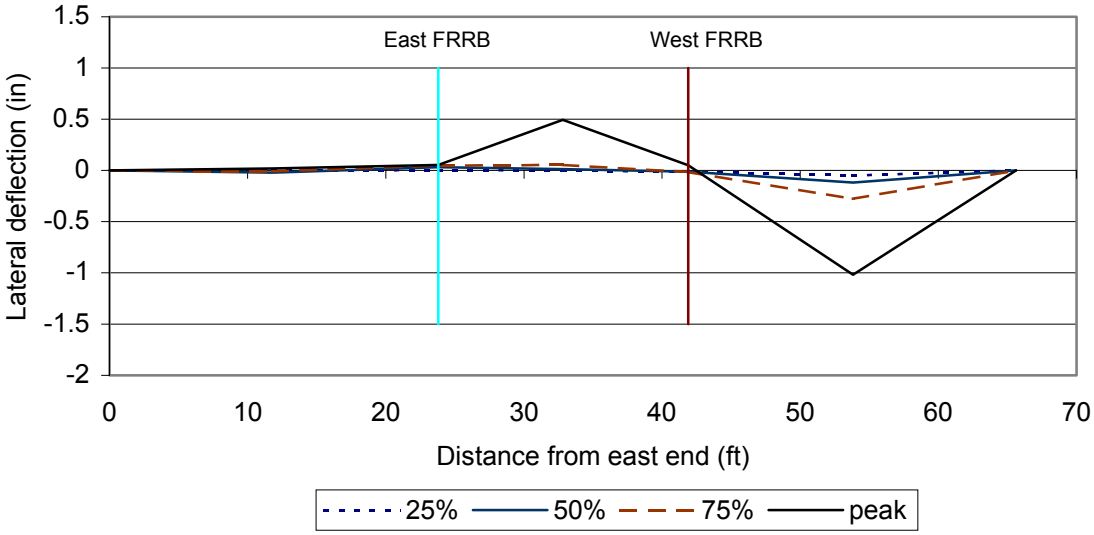

(a) North girder

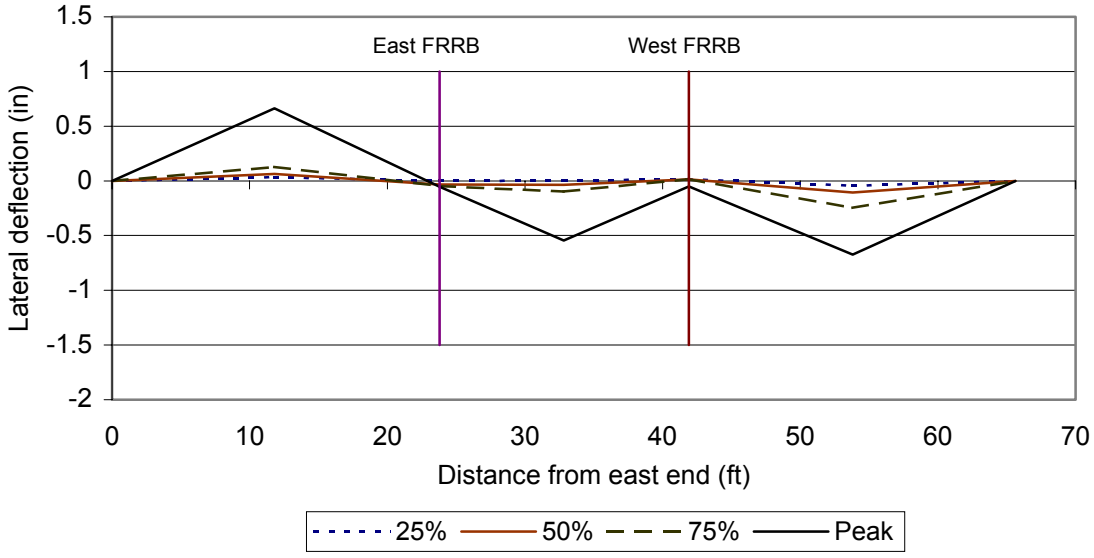

(b) South girder

Figure 26. Girder top flange lateral deflection at different load levels.

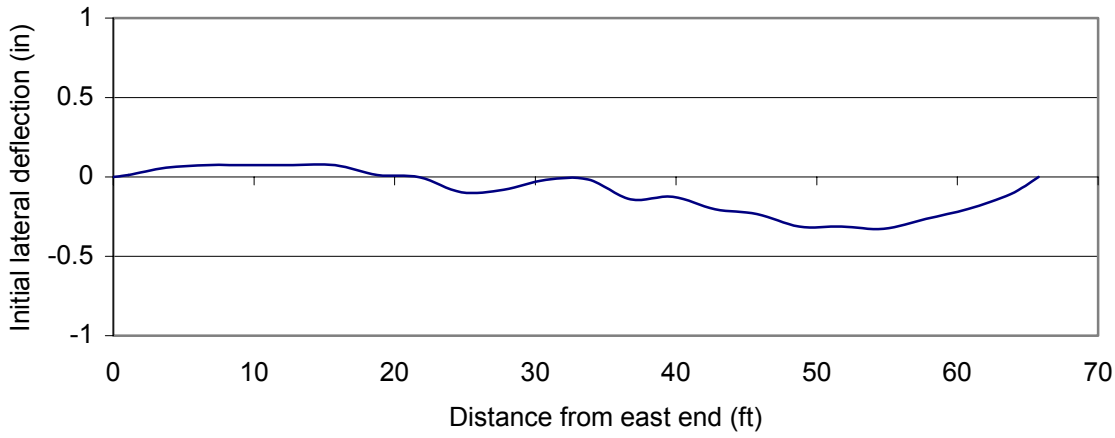

(a) North girder

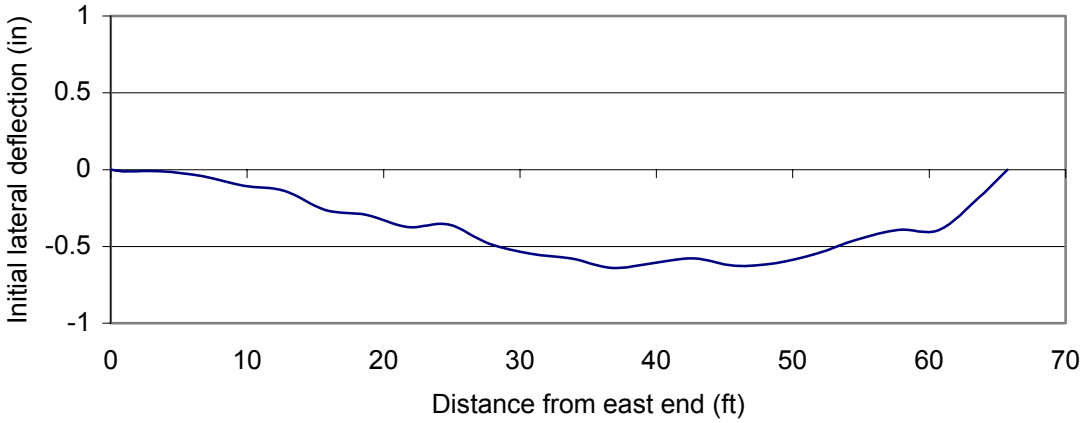

(b) South girder

Figure 27. Girder top flange initial lateral deflection (out-of-straightness).

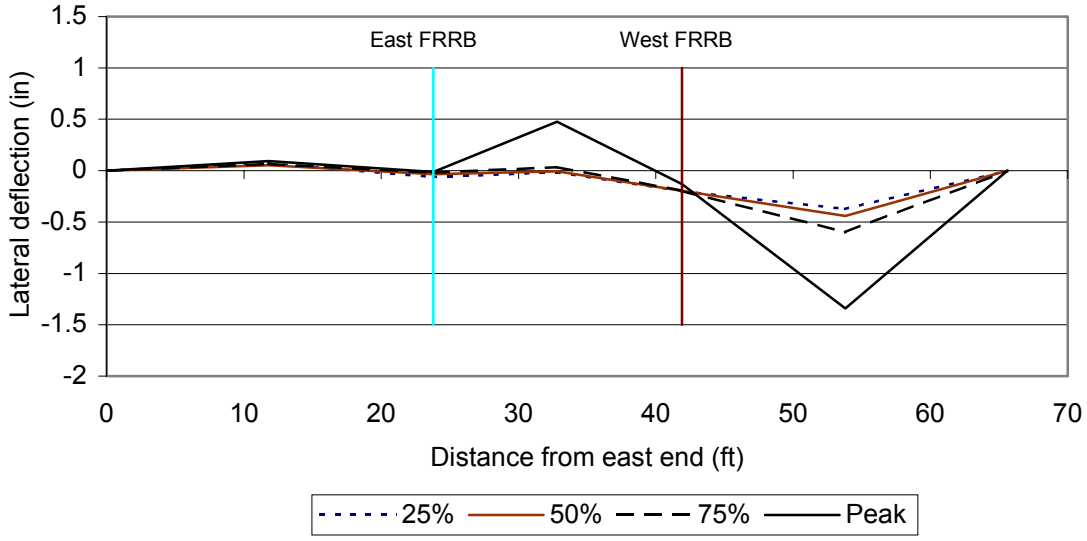

(a) North girder

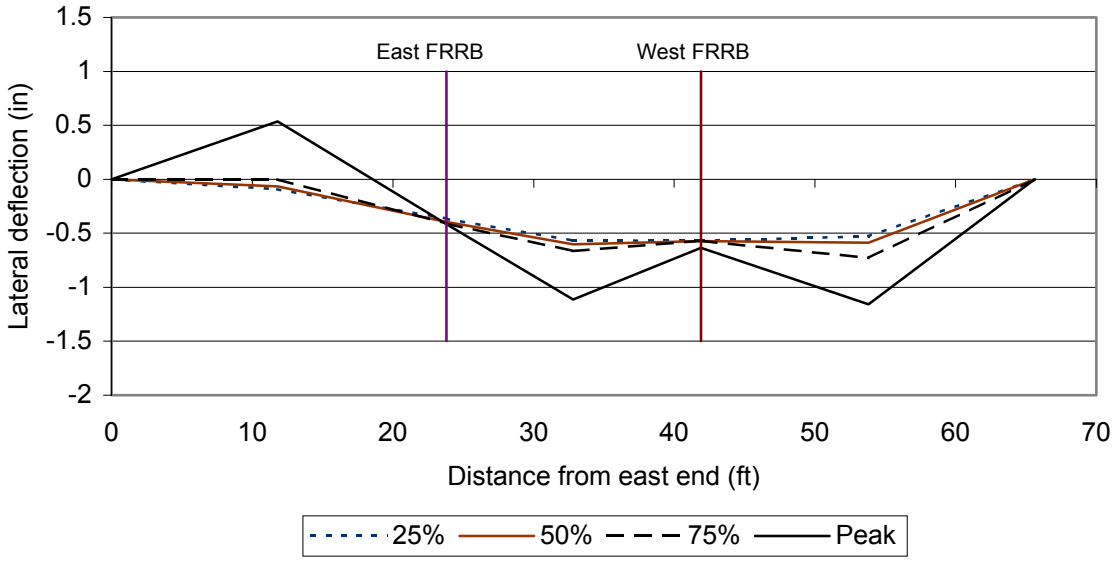

(b) South girder

Figure 28. Girder top flange total lateral deflection at different load levels.

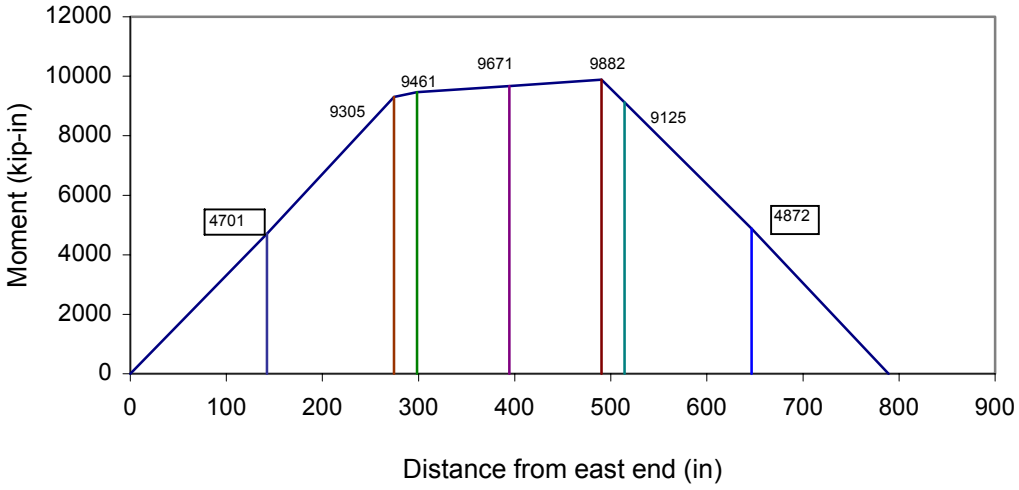

(a) North girder

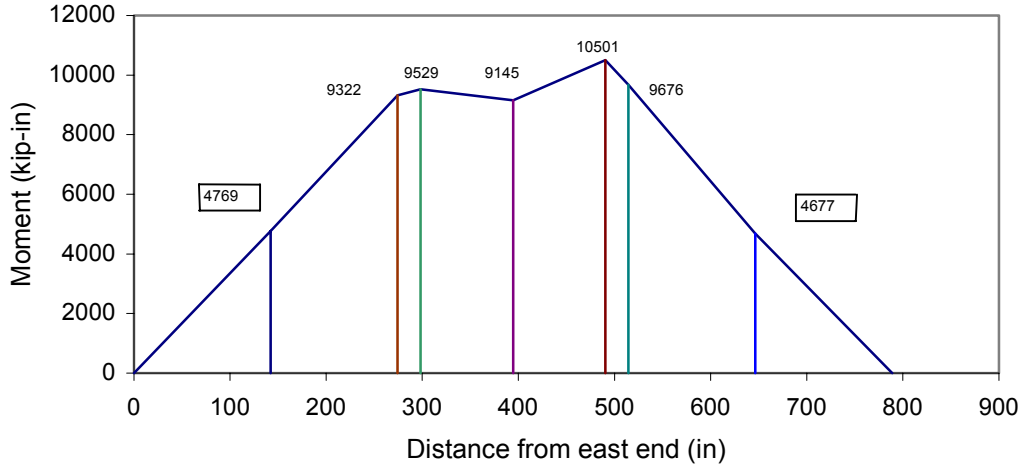

(b) South girder

Figure 29. Girder major principle axis bending moment at peak from Method 1.

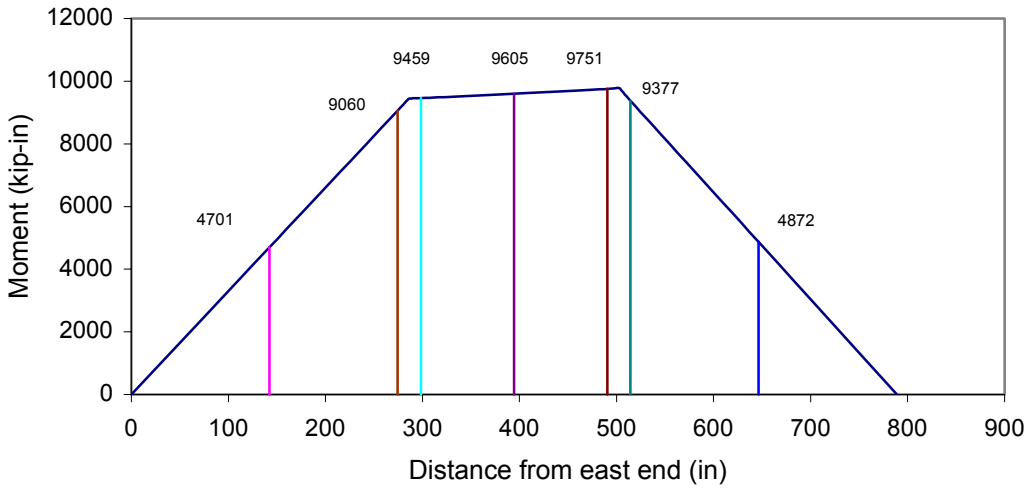

(a) North girder

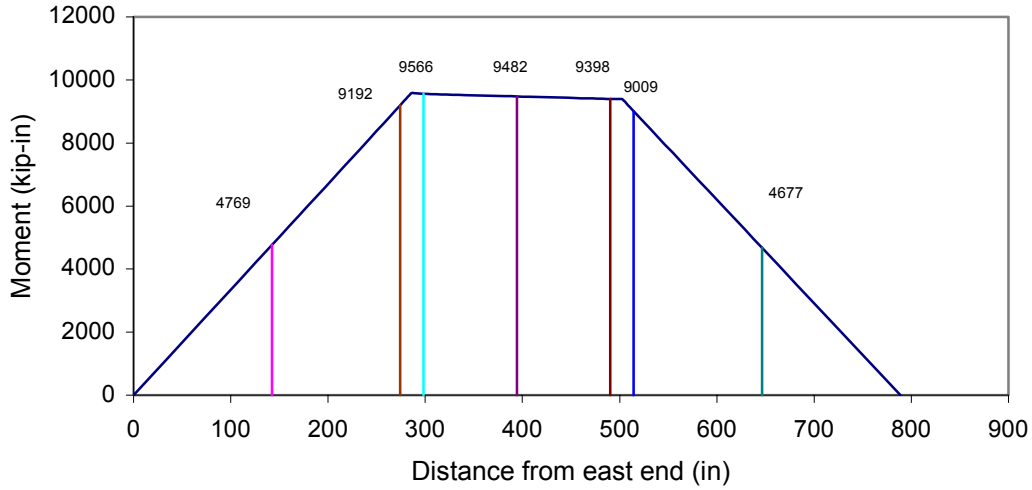

(b) South girder

Figure 30. Girder major principle axis bending moment at peak from Method 2.

6. Summary and Conclusions

This report presents Work Area 5 of the Pennsylvania High Performance Steel (HPS) Bridge Demonstration Project. In particular it focuses on the lateral-torsional buckling of bridge I-girders braced with diaphragms having flange rotational restraint braces (FRRBs). An analysis method for calculating the lateral-torsional buckling moment capacity of I-girders with FRRBs is presented. The results of a large-scale test of a two-girder test specimen are also presented. The properties of the test specimen are summarized, and the lateral-torsional buckling analysis method is used to analyze the test specimen. The test set-up, instrumentation, and test procedure are also summarized. The test results are presented and the analysis results are compared with the test results. Finally, the behavior of the test specimen is compared with the behavior assumed by the analysis method.

The test results show that analysis method presented in the report is effective in determining the lateral-torsional buckling moment capacity of I-girders braced with diaphragms having FRRBs. It is concluded that the lateral-torsional buckling formulas presented in the report, based on those in the AASHTO LRFD bridge design specifications (AASHTO 1998), can be used to predict the inelastic and elastic lateral-torsional buckling moment capacity when an effective length factor, K_b, is introduced into the formulas. The analysis method estimated the lateral-torsional buckling moment capacity of the test specimen within 2%.

FRRBs can provide I-girders with increased lateral-torsional stability compared with traditional bracing methods. Thus, FRRBs can be used to increase the unbraced length while maintaining a fixed lateral-torsional buckling moment capacity, or to increase the lateral-torsional buckling capacity while maintaining a fixed unbraced length. The effective length factor K_b for the test specimen was 0.72 for the inner unbraced lengths, which had an FRRB at each end, and 0.84 for the outer unbraced lengths, which had an FRRB at one end only. These are considered to be typical results. The use of FRRBs with a resulting effective length factor of 0.72 would permit the unbraced length (cross frame or diaphragm spacing) to be increased by 39% without a reduction in the lateral-torsional buckling moment capacity. Further examples of the benefits of using FRRBs are given by Ellis and Sause (1999).

References

AASHTO (1998), *AASHTO LRFD Bridge Design Specifications*, 2nd edition, American Association of State Highway and Transportation Officials, Washington, D.C.

Ellis, C. and Sause, R. (1999), "Minimum Weight HPS Bridge I-girders: Influence of Design Parameters Affecting Fabrication Effort," ATLSS Report No. 99-04, Center for Advanced Technology for Large Structural Systems, Lehigh University, Bethlehem, PA.

Galambos, T. V., (1968), *Structural Members and Frames*, Prentice-Hall, Englewood Cliffs, NJ.

Murphy, S. S. (1997), "Innovative Lateral Bracing of High Performance Steel Highway Bridge I-Girders," M.S. Thesis, Civil and Environment Engineering Department, Lehigh University, Bethlehem, PA.

Salmon, C. G. and Johnson, J. E., (1971), *Design and Behavior of Steel Structures*, Harper & Row, New York.

Sause, R., Abbas, H.H., Wassef, W., Driver, R.G., and Elgaaly, M. (2003) "Corrugated Web Girder Shape and Strength Criteria: Work Area 1, Pennsylvania Innovative High Performance Steel Bridge Demonstration Project," ATLSS Report No. 03-18, Center for Advanced Technology for Large Structural Systems, Lehigh University, Bethlehem, PA.

Sause, R. and Clarke, T.S., (2003), "Bearing Stiffeners and Field Splices for Corrugated Web Girders: Work Area 4, Pennsylvania Innovative High Performance Steel Bridge Demonstration Project," ATLSS Report No. 03-21, Center for Advanced Technology for Large Structural Systems, Lehigh University, Bethlehem, PA.